Neural Network-Based Intelligent Control of Continuous Flow Ohmic Heating Systems for Enhanced Dynamic Performance and Sustainable Food Processing

JAVED, Tasmiyah, LUKE, Leo Pappukutty, ISSA, Walid <http://orcid.org/0000-0001-9450-5197>, SPENDLOVE, James, AKMAL, Muhammad <http://orcid.org/0000-0002-3498-4146>, BREIKIN, Timofei, MILLMAN, Caroline <http://orcid.org/0000-0003-4935-0477>, RASHVAND, Mahdi <http://orcid.org/0000-0002-3767-3028> and ZHANG, Hongwei <http://orcid.org/0000-0002-7718-021X>

Food and Bioprocess Technology (2026) 19:371
https://doi.org/10.1007/s11947-026-04450-7

RESEARCH

Neural Network-Based Intelligent Control of Continuous Flow Ohmic Heating Systems for Enhanced Dynamic Performance and Sustainable Food Processing

Tasmiyah Javed[1] · Leo Pappukutty Luke[1] · Walid Issa[2] · James Spendlove[2] · Muhammad Akmal[2] · Timofei Breikin[2] · Caroline Millman[1] · Mahdi Rashvand[3] · Hongwei Zhang[1]

Received: 28 March 2026 / Accepted: 10 June 2026

Abstract

Continuous flow Ohmic heating (CFOH) is a sustainable thermal processing technology that enables rapid volumetric heating through the electrical resistance of food materials. However, the strong nonlinear coupling between electrical conductivity, temperature, and heat transfer dynamics complicates accurate temperature regulation and stable process operation. This study proposes and evaluates advanced neural network (NN)-based control strategies for nonlinear CFOH systems using nonlinear autoregressive moving average level-2 (NARMA-L2) and model reference control (MRC) architectures. A real-time validated pilot-scale CFOH model implemented in MATLAB/Simulink was utilised to develop, train, and evaluate the controllers under realistic food processing conditions using sweet and sour sauce as the working fluid. The proposed framework integrates dynamic performance analysis, robustness evaluation, energy efficiency assessment, and indirect greenhouse gas (GHG) emission analysis within an integrated evaluation platform. Controller robustness was evaluated under variations in electrical conductivity, flow rate, inlet temperature, sensor noise, and setpoint disturbances. Within the validated simulation framework, the results demonstrate that the NARMA-L2 controller achieved faster dynamic response, reduced settling time, improved stability, zero overshoot, and lower steady-state energy consumption compared to other evaluated strategies. The NN-based controllers also maintained stable performance under varying operating conditions, demonstrating improved adaptability to nonlinear process behaviour. Overall, the proposed NN-based controllers demonstrate strong potential for enhancing process efficiency, operational stability, and sustainability in industrial CFOH applications.

Keywords Continuous flow Ohmic heating (CFOH) · NARMA-L2 controller · Model reference control (MRC) · Nonlinear systems · Energy efficiency · Robustness analysis · Sustainable thermal processing

Introduction

Theglobal food and drink industry (FDI) continues to expand rapidly and is forecasted to expand with a compound annual growth rate (CAGR) of 10.5% until 2029. In the United Kingdom (UK), it holds particular significance as the largest manufacturing sector, generating an annual turnover of £148 billion (Elfadel Haroon, 2024). This industrial growth is accompanied by substantial energy consumption and greenhouse gas (GHG) emissions. Studies have revealed that the food processing system accounts for about 30% of total energy consumption and around 26% of all GHG emissions (Fig.1), as the sector heavily relies on fossil fuels worldwide (Corigliano et al., 2021). In the UK alone, food and drink processing was estimated to consume about 24.6 TWh of energy and emit approximately 9.1 million tonnes of CO per year (Gowreesunker et al., 2026).

The food- processing industry is one of the major contributors to GHG emissions and industrial energy consumption. The sector's heavy reliance on conventional heating methods not only exacerbates environmental degradation but also places immense pressure on energy resources. In response,

✉ Hongwei Zhang
h.zhang@shu.ac.uk

[1] Advanced Food Innovation Centre (AFIC), Sheffield Hallam University, Sheffield, United Kingdom

[2] School of Engineering and Built Environment, Sheffield Hallam University, Sheffield, United Kingdom

[3] Centre for Business and Industry Transformation, Nottingham Trent University, Nottingham, United Kingdom

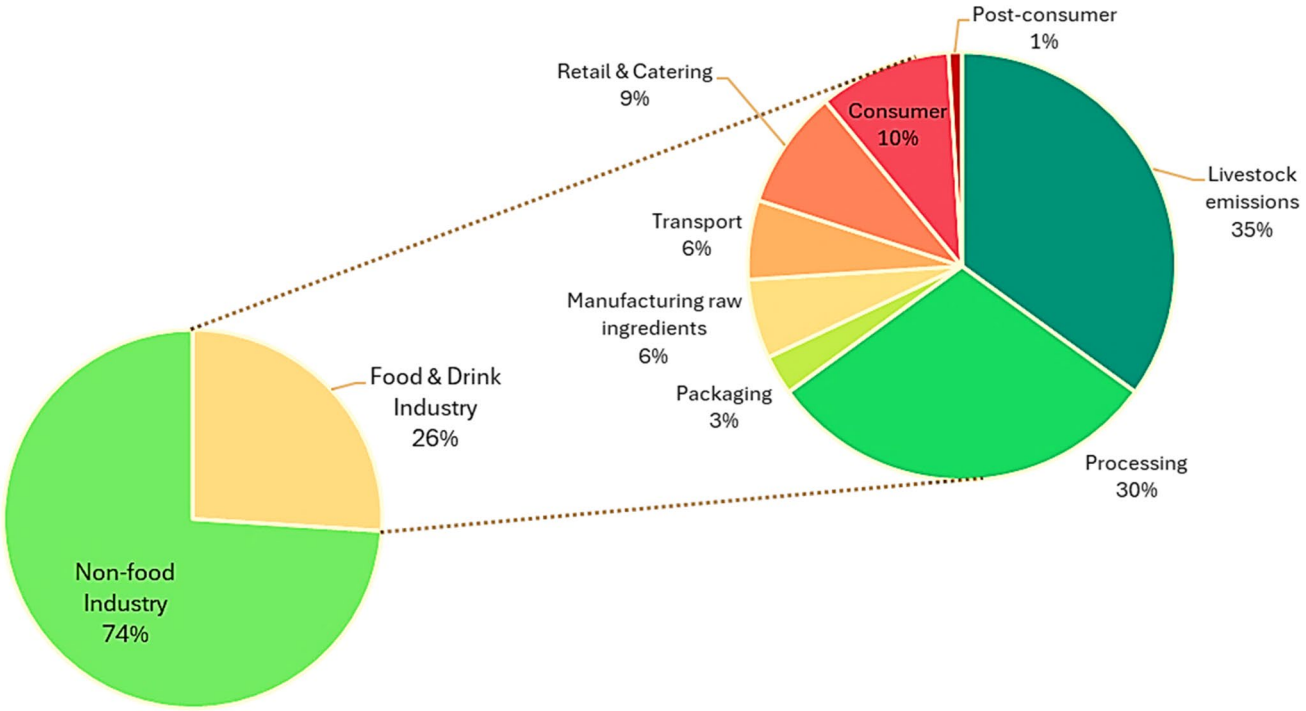

Fig. 1 Breakdown of GHG emissions in the UK food and drink industry

the UK's food and drink federation (FDF) has aimed to achieve net zero emissions by 2040 (Elfadel Haroon, 2024). This sector-wide target necessitates the widespread adoption of greener, more efficient processing technologies in food manufacturing. Consequently, considerable research is now focused on developing alternative and advanced technologies for sustainable food processing. CFOH is an emerging industrial food- processing technology characterised by direct volumetric heating, which substantially minimises thermal losses and improves temperature uniformity throughout the process. These advantages enhance operational efficiency and reduce the carbon footprint by eliminating dependence on fossil fuel-–based thermal energy sources, thereby positioning CFOH as a highly sustainable and environmentally friendly processing technology. Nevertheless, the successful implementation of CFOH requires advanced automation systems and intelligent control strategies to maintain operational stability, optimise energy consumption, ensure product quality and further minimise environmental impacts during industrial-scale processing operations.

Advanced control strategies also contribute to industrial decarbonisation by reducing indirect greenhouse gas emissions associated with energy use. These assertions are supported by previous studies demonstrating that enhanced process control improves both control accuracy and overall system efficiency in nonlinear thermal systems (Alamirew et al., 2017).

Gethchell in the 1930 s was among the first to stress the importance of controlling Ohmic heating (OH) parameters (Bachi et al., 2021). In those early implementations, control schemes were often rudimentary. Simple on/off thermostatic controllers were common in thermal systems due to their simplicity, but they often led to oscillatory temperature swings and overshoot.Vandoren, (1998) noted that purely open-loop control of OH suffers from inaccuracy because the system cannot correct for disturbances or system errors (Çelik 2026). Stirling, (1987) outlined the key control requirements for an Ohmic heater, noting that the controller must maintain the outlet temperature despite variations in flow rate, incoming product temperature, and power input (Chebbi 2024). These early limitations underscored the need for more sophisticated control strategies as OH applications expanded.

Subsequent developments introduced closed-loop feedback control to OH systems to improve accuracy and operational robustness. During this period a prevalent approach was the PID controller which had become ubiquitous in industrial heating control. This is because it is straightforward to understand and easy to implement and provides satisfactory performance in linear or slowly changing systems. Numerous studies have been conducted on PID theory tuning techniques and practical applications in closed-loop systems. Research by Skudder & Stirling, (1992) described an OH system where a microprocessor continuously adjusted electrical power based on feedback, comparing the desired

output temperature with the measured output and modulating the transformer voltage accordingly (Corigliano et al. 2025). This early PID-controlled Ohmic heater marked a transition to closed-loop automation. Research by Li & Li, (2019) demonstrated that basic temperature feedback, along with an integration of appropriate proportional control gain, can effectively regulate applied voltage in an Ohmic heater, reducing steady-state error and enhancing stability (Dinç & Erentürk, 2024). Compared to on/off control, PID provided smoother control action and reduced oscillations, but it still faced challenges due to the intrinsic nonlinearity of OH. Temperature-dependent changes in the electrical conductivity of the product can significantly alter the system dynamics during operation, meaning that a fixed PID tuning may exhibit suboptimal performance in the presence of substantial nonlinearities and evolving operational parameters (Dong 2017). Hence, PID-controlled systems are optimised for a specific operating point and exhibit no adaptability to fluctuations in system performance.

Therefore, in systems such as CFOH that are characterised by significant nonlinearities, time varying electrical characteristics, and interrelated thermal-electrical dynamics, the limitations of fixed gain PID controllers become increasingly evident. Traditional controllers are unable to adapt to varying operational conditions, resulting in frequent temperature fluctuations, longer settling times, and increased energy consumption. This performance decline not only diminishes product quality and process safety but also undermines energy efficiency and the environmental advantages of sustainable thermal processing.

Consequently, researchers in thermal processing have observed these shortcomings and compared PID to more adaptive controls. A clear example is found in Ohmic heating control experiments, where Dinc and Erentürkn (2024) designed both a PID and a fuzzy logic controller (FLC) for an OH system and compared their performance. The PID was tuned for optimal response at a given operating point, yet the FLC significantly outperformed it, achieving more stable temperature control, faster settling with no overshoot and generally more powerful control action (Fakinle 2019). This indicates that the fixed gain PID could not cope as well with the system's nonlinear behaviour, whereas the rule-based fuzzy controller could adapt its output to maintain stability. Such findings mirror results in other heating applications; for instance, fuzzy logic has also proven superior to PID in maintaining precise temperature on an induction-heating cooker, especially under varying conditions (Food & Drink Federation, Industry at a Glance, n.d.).

Likewise, conventional PID loops in milk pasteurisation units often struggle with the process's inherent time delays and time-varying dynamics, prompting the need for more advanced tuning or control schemes (Gowreesunker et al. 2018). These examples underscore that if operating conditions are steady and well characterised, PID control works, but in nonlinear, time-varying environments typical of food processing, its performance and efficiency can be suboptimal. These issues emphasise the necessity of sophisticated control methodologies capable of learning system dynamics and adapting in real time to address nonlinear process behaviour. Artificial neural network (ANN)-based intelligent control approaches have emerged as promising solutions for handling complex nonlinear systems, owing to their capability to learn system dynamics without requiring explicit mathematical models. This enhances their robustness, adaptability, and precision in managing energy-intensive industrial operations (Hagan 1999).

Recent NN-based control technologies have shown effectiveness in handling nonlinearities, uncertainties, and disturbances in complex systems. NN-based adaptive fault-tolerant control approaches have been successfully applied to compensate for modelling uncertainties, external disturbances, and actuator faults while maintaining prescribed tracking performance. For example, Hui and Yuan developed a neural-network-based adaptive fault-tolerant control framework using radial basis function neural networks (RBFNNs) to estimate lumped uncertainties and actuator faults in a modular high-temperature gas-cooled reactor system, achieving improved robustness and tracking accuracy under uncertain operating conditions (Hui & Yuan 2022). Similarly, advanced adaptive sliding mode and intelligent nonlinear control strategies have been proposed for robust power-level regulation and disturbance rejection in nonlinear nuclear power systems (Hui & Yuan 2022). In addition, Zhang et al. developed a neural direct adaptive active disturbance rejection controller (NDADRC) for electro-hydraulic servo systems, where neural networks were integrated with active disturbance rejection control to enhance adaptability, tracking performance, and disturbance compensation capability under nonlinear dynamics and parameter uncertainties (Javed 2025). These studies highlight the growing importance of intelligent learning based control architectures for complex thermal and nonlinear dynamic systems, where conventional fixed-gain controllers may exhibit degraded performance under varying operating conditions and process nonlinearities.

S, intelligent and nonlinear control systems, such as the NARMA-L2 controller, are designed to handle complex dynamics by compensating for inherent nonlinearities using trained models. In a variety of control systems, such as steel rolling mills, shell and tube heat exchangers, continuous stirred tank reactors (CSTRs) and chemical process models, the NARMA-L2 architecture has proven to be resilient to disturbances and to have better tracking performance than conventional controllers in nonlinear settings (Li & Li 2019; Narendra & Mukhopadhyay 1997; Narendra & Parthasarathy 2002). Using NN-based models of process dynamics,

these controllers generate control actions that improve the linearity of the closed-loop behaviour. This facilitates faster responses and reduced overshoot responses from highly dynamic systems. The enhanced control performance is particularly beneficial for CFOH systems, since faster and precise temperature regulation directly influences energy efficiency, operational stability and the sustainability of the thermal processing operation.

Leveraging the advantages of intelligent nonlinear controllers, another effective model-based control strategy for managing complex and nonlinear industrial processes is represented by MRCs. The closed loop's behaviour is precisely specified by MRC using a reference model. Rather than merely employing pre-established control heuristics, MRC techniques construct the controller so that the system's actual output corresponds to the response of a reference model, which illustrates the ideal behaviour of the system. By continuously adjusting the control action as necessary, MRC structures can improve tracking and disturbance rejection performance by comparing the plant output to the output of the reference model. Systems having dynamic uncertainties or nonlinearities are particularly affected by this approach. One prominent example is the reduction of power system oscillations using an NN-based MRC architecture. Reduced integral square error indices in simulation studies indicate that the MRC's model matching objective significantly enhances damping performance when compared to traditional proportional-integral (PI) control in this context (Oluwole-ojo 2023). Controller frameworks of this type demonstrate how model-referenced methods can maintain robust control over complex industrial processes while ensuring that the system's actual outputs meet the dynamic targets that were intended. In CFOH, the application of MRC techniques enhances temperature regulation, optimises energy efficiency, and amplifies the advantages of advanced control technology. Similar temperature estimation and control challenges are also observed in other electrically heated manufacturing systems beyond food processing. For instance, Chebbi et al. (Oluwole-ojo 2024) investigated substrate temperature estimation and control in advanced metal-organic chemical vapour deposition (MOCVD) processes for superconductor manufacturing. Their study highlights the importance of accurate thermal modelling and advanced control strategies in systems characterised by nonlinear dynamics and strong thermal–electrical coupling. These challenges are closely aligned with those encountered in CFOH, further supporting the need for robust and intelligent control approaches.

In the context of OH, adaptive controllers are highly beneficial because food properties (density, specific heat, conductivity) can change with temperature or as composition evolves (e.g., starch gelatinisation in a sauce). An adaptive algorithm can revise the control law on the fly to retain stability and performance despite these changes. However, ensuring stability during adaptation is a key challenge; the system must be carefully designed so that parameter updates improve performance without introducing oscillations. This often requires a robust estimation of the current system parameters, which itself can be sensitive to sensor noise or abrupt disturbances. Sensor inaccuracies pose a problem here: an adaptive controller updating its model based on noisy temperature readings might mistune itself. Thus, high-quality sensing and filtering are critical for successful adaptive control in Ohmic heating. In the realm of OH, such hybrid and intelligent controllers are still an active research frontier, but their potential is significant.

Implementing advanced controllers enhances operational efficiency while simultaneously promoting environmental sustainability through improved energy utilisation. These intelligent control systems utilise reduced electricity consumption, thereby diminishing GHG emissions not directly attributable to them. This is particularly applicable in regions where fossil fuels are utilised for energy production. CFOH processes can maintain a consistent temperature and ensure the quality of items through appropriate control systems. This also assists enterprises in conserving funds while achieving their objectives for minimising their carbon impact and decarbonisation. Additionally, the capacity to dynamically optimise controller behaviour, as demonstrated by validated models and real-time CFOH pilot tests, highlights the growing importance of control engineering at the intersection of sustainability and industrial automation objectives (Paul & Chokkadi 2016).

Based on the reviewed literature, control strategies for Ohmic heating systems and other thermal systems have evolved throughout time, from straightforward open-loop and on/off controls to traditional PID controls and, more recently, intelligent, adaptive and hybrid control architectures. Although fixed-gain PID controllers are frequently employed in industry, they perform poorly in situations with numerous nonlinearities and fluctuating operational parameters. These systems do not respond to shifts in system performance since they are tuned for a particular operating point (Dong 2017). Fuzzy logic and adaptive schemes are examples of intelligent controllers that have shown improved stability and robustness.

However, many existing approaches either focus primarily on temperature regulation without explicitly optimising dynamic performance metrics or impose significant design complexity and training dependencies. Further, while energy-efficient control is becoming increasingly popular, there are limited studies that systematically link improvements in controller performance to energy efficiency and the consequent drop in indirect greenhouse gas emissions associated with electrical energy use. Comprehensive comparative studies evaluating both traditional and advanced

intelligent controllers in a single framework for CFOH that consider control performance across several matrices and sustainability are conspicuously lacking. This disparity highlights how crucial it is to implement and evaluate novel control systems that can maintain precise temperature control while reducing response and settling times, overshoot, and control error. These developments are crucial for ensuring the safety and quality of food, but they are also crucial for improving energy efficiency and, eventually, reducing GHG emissions. These developments will increase the sustainability of thermal processing systems.

This study presents a unified framework for comparing PID and advanced NN-based NARMA L2 and MRC controllers using a real-time validated pilot-scale CFOH model developed in MATLAB/Simulink. The framework integrates dynamic performance, robustness, energy efficiency, and sustainability assessment under realistic thermal processing conditions, providing a comprehensive platform for evaluating intelligent control strategies for nonlinear food processing systems.

Pilot-Scale CFOH System and Experimental Data Acquisition

A pilot-scale CFOH system was used for experimental data acquisition, with the working fluid being a sweet-and- sour sauce exhibiting a conductivity of 0.6 S/m. A conductivity meter, the Apera Instruments Premium Series PC60 multiparameter pocket tester kit, was used to measure conductivity. A pump connects the infeed tank to the Ohmic heating chamber, ensuring continuous fluid flow into the heating chamber.

The Ohmic chamber contains three vertically arranged electrodes, spaced 0.6 and 0.8 m apart, encased in insulating layers. High voltage (HV) is applied to the central electrode, creating two heating zones: one between the infeed electrode and the central electrode (labelled as Electrode 2 in Fig. 2) and the other between the central electrode and the outfeed electrode. A thyristor operating in phase-angle control mode regulates the power supplied to the fluid by adjusting the voltage on the primary winding of the transformer. A programmable logic controller (PLC) governs this thyristor configuration; however, it can additionally be operated via Sheffield Hallam University's PC-based open-loop control system.

The chamber operates autonomously and is equipped with an integrated PLC-human machine interface (HMI) that enables user control of the power supply. The system accommodates large power levels (up to 12 kW from a 63 A supply) and a range of fluid conductivities (from 0.1 to 4 S/m), making it suitable for a wide range of food products. A crucial aspect of the system is its continuous monitoring of temperature at multiple locations. Thermocouple gauges measure the temperature of the infeed TC1 and the outfeed TC2. Fibre optic probes provide high-precision temperature measurements. FT1 and FT2 monitor the outlet temperature, while FT3 and FT4 assess the temperature within the heating chamber.

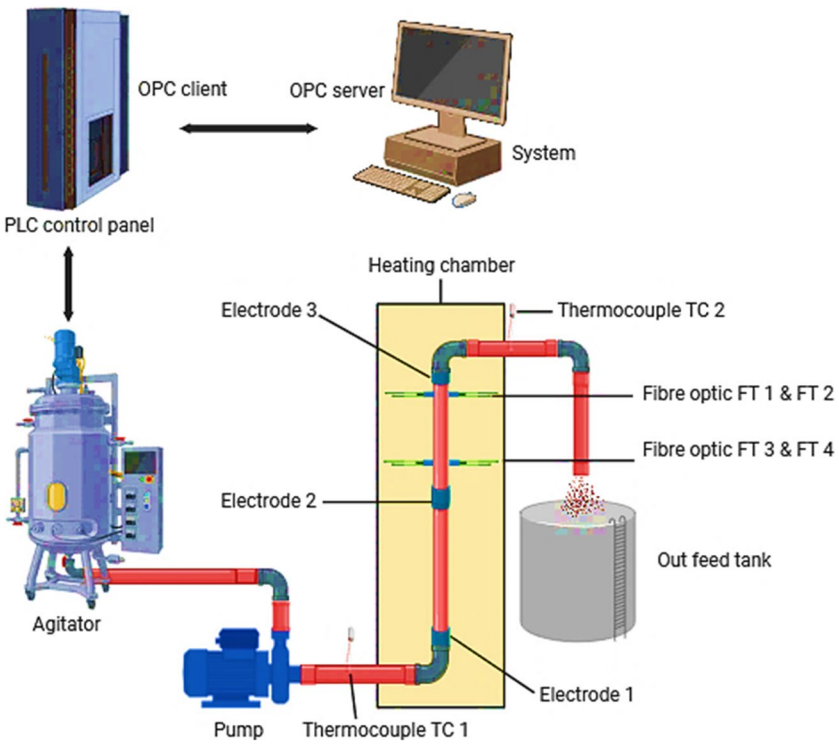

Fig. 2 Pilot-scale CFOH system used for experimental data acquisition

The pump is initiated by activating the Pump Start button or via the control PC. The fluid is subsequently pumped upward, filling the applicator beyond the outfeed electrode. The pump speed can be adjusted as required. During operation, key parameters such as voltage, current, power consumption, thermocouple measurements, fibre optic temperature readings and flow rate are continuously monitored. The heating process is completed when the fluid exits the heating chamber and reaches the outfeed collection tank at the appropriate temperature.

Overall, the pilot-scale CFOH system provides a well-controlled and adaptable platform for investigating thermal processing under real-time operating conditions. With accurate power regulation, flexible flow control and multi-point temperature monitoring, the system enables precise characterisation of heat transfer behaviour and process dynamics. This comprehensive experimental setup ensures reliable data acquisition, supporting the development and implementation of advanced data-driven NN-based controllers.

Open Platform Communications (OPC)-Based Communication Framework

Comprehensive data covering the entire operational process of the CFOH system was collected for the training, testing and validation of the NN-based controllers. Throughout the operation, critical parameters were continuously monitored and recorded. An OPC server facilitated data collection by enabling the PLC controlling the Ohmic heater to communicate and exchange data with another computer in the laboratory. This configuration enabled the implementation of both conventional and advanced model-based control techniques within the MATLAB/SIMULINK framework.

The OPC server and client protocol provide real-time data transmission and reception over a local area network (LAN). The KEPServerEX OPC server was configured to communicate with the PLC via Ethernet through the PLC's Ethernet module. This configuration enables the lab PC to read from and write to the PLC, monitor data in real time and store information. This setup allows the use of both basic and advanced controllers, facilitating precise operational control. The PLC transmitted input/output (I/O) tags to the OPC server, allowing MATLAB to communicate with the PLC for control and monitoring purposes.

Conventional PID Controller Design and Benchmark Comparison

To evaluate the effectiveness of the proposed NN-based control strategies, their performance was compared with that of a PID controller, which combines proportional, integral and derivative actions to achieve the desired dynamic system response in thermal processing applications. The Ziegler–Nichols (ZN) tuning approach was employed to design and tune the PID controller. This method provides a systematic framework for determining optimal controller settings based on the system's response to variations. The tuning procedure resulted in proportional, integral and derivative gains of $k_p = 1.6$, $k_i = 0.02$ and $k_d = 0$, respectively.

The selected configurations ensure the system operates efficiently, responds promptly and maintains a minimal steady-state error for the specified setpoint. The Ziegler–Nichols tuning method was selected in this study to provide a standard and reproducible conventional PID benchmark for comparison with the NN-based controllers. Although Ziegler–Nichols' tuning is known to produce a relatively aggressive response in some nonlinear or time-delay systems, it remains a widely recognised tuning method in classical process control and provides a transparent basis for controller comparison. The objective of including the ZN-PID controller was not to present it as the optimal PID strategy, but to establish a conventional fixed-gain control baseline under the same CFOH operating conditions. This enables fair evaluation of the relative advantages of NARMA-L2 and MRC controllers in terms of response speed, overshoot, settling behaviour and energy efficiency.

General Design Methodology of NeuralNetwork–Based Controllers for CFOH

Neural network–based controllers were developed to address the strongly nonlinear and coupled thermal–electrical dynamics of the CFOH process. Unlike conventional fixed-parameter controllers, neural network–based control strategies can learn nonlinear input–output relationships directly from process data, enabling improved adaptability and dynamic response under varying operating conditions.

The controller development procedure consisted of several stages, including experimental data acquisition, nonlinear plant identification, neural network training, validation, controller implementation and robustness evaluation. Real-time experimental input–output data were collected from the pilot-scale CFOH system using sweet and sour sauce under varying operating conditions to ensure sufficient excitation of the process dynamics. The collected dataset included thyristor voltage inputs, outlet temperature responses and transient operating conditions representative of practical food processing environments.

The neural network architecture and controller parameters were selected through systematic evaluation of multiple network configurations. The number of delayed inputs and outputs was determined based on the dominant thermal dynamics, transport delay and memory effects of the CFOH system. Similarly, the number of hidden neurons was selected by analysing prediction accuracy, regression performance, convergence behaviour and model generalisation

capability. Networks with insufficient neurons exhibited poor nonlinear approximation, whereas excessively large networks increased computational complexity and the risk of overfitting. The final selected architecture provided a balance between prediction accuracy and computational efficiency.

The neural networks were trained using the Levenberg–Marquardt optimisation algorithm due to its fast convergence characteristics for medium-sized nonlinear regression problems. To improve generalisation and minimise overfitting, the dataset was divided into training, validation and testing subsets. The validation dataset was used to monitor network performance during training, while the independent testing dataset was used to evaluate final prediction capability.

Since the proposed controllers are designed for nonlinear data-driven system representations, deriving a strict global analytical stability proof is difficult due to the complex nonlinear approximation characteristics of neural networks. Therefore, controller stability and robustness were evaluated practically through extensive closed-loop simulations and robustness analyses under varying conductivity conditions, flow-rate disturbances, inlet-temperature variations, sensor noise and set-point changes. These procedures ensured that the developed NN-based controllers achieved accurate nonlinear modelling, reliable prediction capability and stable control performance suitable for practical CFOH applications.

Design of Nonlinear Autoregressive Moving Average Level-2 (NARMA-L2) controller for Continuous Flow Ohmic Heater (CFOH)

NARMA-L2 control and feedback linearisation are used to describe the NN controller discussed in this section. When the plant model has a particular form, it is called feedback linearisation (companion form). When the same form can be used to approximate the plant model, this is referred to as NARMA-L2 control. The main concept of this type of control is to cancel out the nonlinearities to convert nonlinear system dynamics into approximately linear dynamics (Richardson 2001).

This section explains the companion form system concept and illustrates the application of an NN to identify this model. It subsequently clarifies the use of the identified NN model for controller development. Figure 3 illustrates the operation of the NARMA-L2 controller.

Identification of NARMA-L2 Model

The first step in developing the NARMA-L2 controller is to identify the nonlinear input–output behaviour of the CFOH system. The general nonlinear autoregressive moving average model represents the system dynamics using an unknown nonlinear mapping denoted by $N[.]$. In the present study, $N[\cdot]$ describes the relationship between the thyristor voltage input and the outlet temperature output of the CFOH system.

Specifically, it maps the current and delayed input values, together with delayed outlet temperature values, to the future outlet temperature. Therefore, $N[\cdot]$ characterises the complete nonlinear plant dynamics, including thermal inertia, transport delay, electrical heating behaviour and the nonlinear relationship between temperature and electrical conductivity.

The general one-step-ahead nonlinear plant model is written as follows:

$$y(k+1) = N[y(k), y(k-1), \ldots y(k-n+1), u(k), u(k-1), \ldots u(k-m+1)] \quad (1)$$

Where $y(k+1)$ is the one-step-ahead outlet temperature, $y(k), y(k-1), \ldots, y(k-n+1)$ are the current and delayed outlet temperature values and $u(k), u(k-1), \ldots, u(k-m+1)$ are the current and delayed thyristor input values. The parameters n and m represent the number of delayed output and input terms used to describe the memory of the system. For predictive control, this one-step-ahead representation is extended to a d-step-ahead prediction, denoted as $y(k+d)$. Thus, $y(k+d)$ represents the predicted system output at the

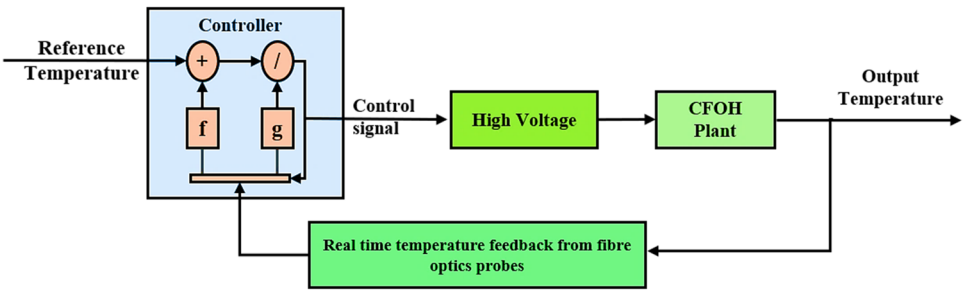

Fig. 3 Working of the NARMA-L2 controller

future prediction horizon and is used in the NARMA-L2 control law to calculate the control input required for reference tracking.

To ensure the system output follows a reference trajectory $y(k+d) = y_r(k+d)$, the next step is to formulate a nonlinear controller with the following structure:

$$u(k) = G[y(k), y(k-1), \ldots y(k-n+1), y_r(k+d), u(k-1), \ldots u(k-m+1)] \quad (2)$$

The issue with employing this controller is that training a neural network to develop the function *G*for minimising mean square error necessitates the utilisation of dynamic backpropagation (Skudder 1992; Stirling 1987). This can be computationally intensive. To reduce this complexity, the NARMA-L2 structure reformulates the nonlinear plant model into a form more suitable for controller implementation.

A proposed approach by Narendra and Mukhopadhyay is the use of approximate models to depict the system (Uddin 2019). This part utilises a controller founded on the NARMA-L2 approximation model.

For NARMA-L2 control, the general nonlinear function $N[\cdot]$ is approximated in an affine-in-control form. This approximation separates the predicted output into two components: an input-independent nonlinear component and an input-dependent nonlinear gain component. The NARMA-L2 model is expressed as follows:

$$\hat{y}(k+d) = f[y(k), y(k-1), \ldots y(k-n+1), u(k-1), \ldots u(k-m+1)] + g[y(k), y(k-1), \ldots y(k-n+1), u(k-1), \ldots u(k-m+1)] \cdot u(k) \quad (3)$$

The predicted output of the NARMA-L2 model is represented by $\hat{y}(k+d)$, where $\hat{y}(k+d)$ denotes the predicted outlet temperature of the CFOH system at d-steps ahead in time. The prediction is generated using the neural-network-identified nonlinear plant model based on previous input–output data of the system. In this expression, $f[\cdot]$ and $g[\cdot]$ are nonlinear functions identified using neural-network training from the experimentally obtained CFOH input–output data. The function $f[\cdot]$ represents the autonomous part of the plant dynamics. It predicts the future outlet temperature contribution caused by the previous outlet temperatures and previous input values, excluding the direct effect of the current control input. The function $g[\cdot]$ represents the nonlinear input-gain function. It determines how the current control input $u(k)$ influences the future outlet temperature. Thus, $g[\cdot]u(k)$ represents the control-dependent part of the predicted output.

The relationship between the general nonlinear function $N[\cdot]$ and the NARMA-L2 functions $f[\cdot]$ and $g[\cdot]$ is important for understanding the controller formulation. The function $N[\cdot]$ represents the complete nonlinear input–output mapping of the CFOH system. However, this general nonlinear form is not convenient for deriving an explicit control law, because the current control input may appear inside the nonlinear function. Therefore, the NARMA-L2 method approximates $N[\cdot]$ using an affine-in-control structure:

$$N[\cdot] \approx f[\cdot] + g[\cdot]u(k) \quad (4)$$

In this approximation, $f[\cdot]$ represents the part of the nonlinear dynamics that is predicted from the past input–output history, while $g[\cdot]$ represents the nonlinear gain through which the current control input affects the future output. Therefore, $f[\cdot]$ and $g[\cdot]$ are not separate physical models, but two neural-network-identified components of the original nonlinear plant mapping $N[\cdot]$. It should be noted that the decomposition of a general nonlinear function $N[\cdot]$ into $f[\cdot]$ and $g[\cdot]$ is not necessarily unique. In this study, $f[\cdot]$ and $g[\cdot]$ are therefore not treated as unique analytical solutions. Instead, they are determined as data-driven approximations through neural-network training. The network parameters are adjusted to minimise the error between the measured outlet temperature and the predicted outlet temperature over the experimentally collected CFOH dataset. The resulting $f[\cdot]$ and $g[\cdot]$ functions correspond to one valid approximation that satisfies the NARMA-L2 structure and provides accurate prediction within the operating region represented by the data.

To ensure that the identified functions are reliable and not simply the result of a non-unique, arbitrary decomposition, the dataset was divided into training, validation and testing subsets. The training data were used to adjust the neural network weights, the validation data were used to monitor generalisation and reduce overfitting and the independent testing data were used to evaluate the final model. Therefore, although the mathematical decomposition is not unique, the selected $f[\cdot]$ and $g[\cdot]$ are justified by their prediction accuracy, validation performance and suitability for realisable NARMA-L2 controller implementation.

This model is presented in companion form, wherein the subsequent controller input u(k) is excluded from the nonlinearity. This form allows for the determination of the control input that enables the system output to align with the reference $y\ (k+d) = y_r\ \ (k+d)$. The resulting controller would have the following form:

$$u(k) = \frac{y_r(k+d) - f[y(k), y(k-1), \ldots, y(k-n+1), u(k-1), \ldots, u(k-n+1)}{g[y(k), y(k-1), .., y(k-n+1), u(k-1), \ldots, u(k-n+1)} \tag{5}$$

Employing this equation directly may lead to realisation issues, as it necessitates determining the control input $u(k)$ concurrently with the output $y(k)$. Therefore, the model was utilised.

$$y(k+d) = f[y(k), y(k-1), \ldots y(k-n+1), u(k), u(k-1), \ldots u(k-n+1)] + g[y(k), \ldots y(k-n+1), u(k), \ldots u(k-n+1)] \cdot u(k+1) \tag{6}$$

Where $d \geq 2$. Figure 4 shows the structure of a neural network representation.

Overall, the NARMA-L2 framework provides an effective nonlinear control formulation for the CFOH system by combining neural network–based plant identification with feedback linearisation principles. By separating the nonlinear plant dynamics into autonomous and control-dependent components, the controller can explicitly compute the control action required for accurate reference tracking while compensating for the inherent nonlinearities of the process.

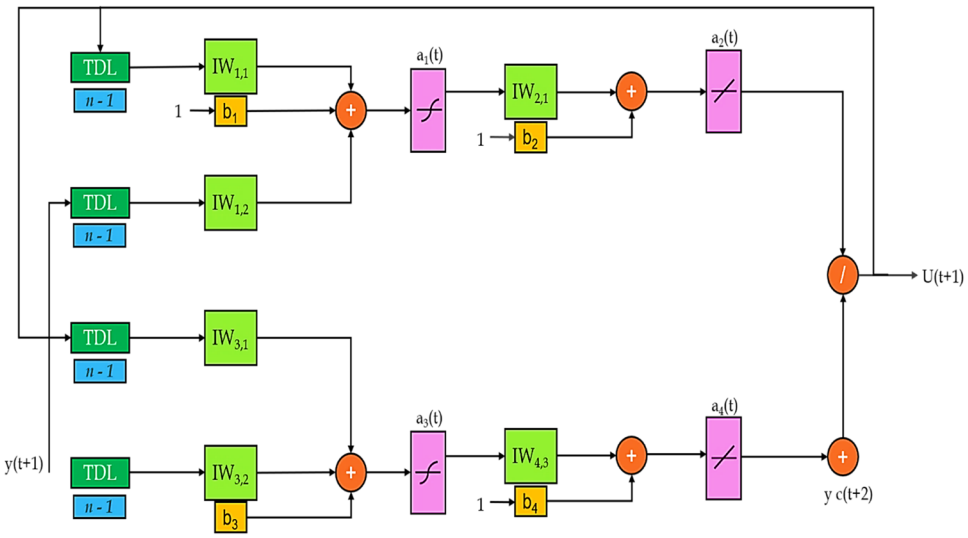

Fig. 4 Structure of neural network representation

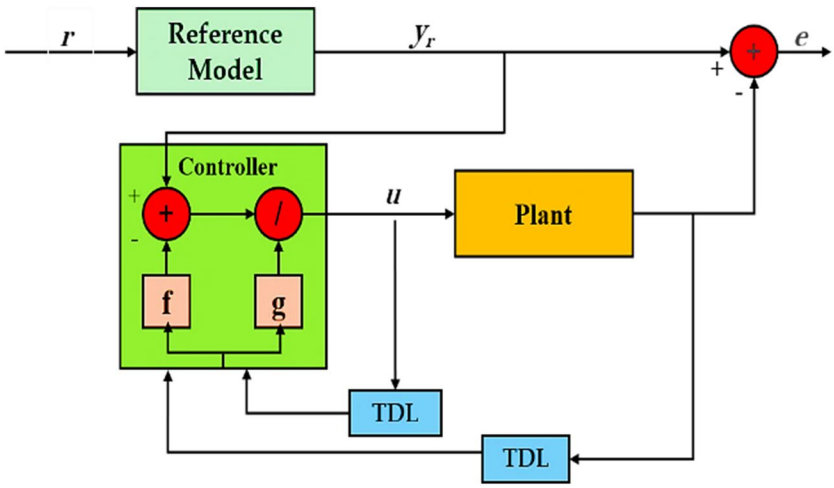

Fig. 5 Block diagram of NARMA-L2 controller

NARMA-L2 Control Law

The controller is derived using the NARMA-L2 model:

$$u(k+1) = \frac{y_r(k+d) - f[y(k), y(k-1), \ldots., y(k-n+1), u(k-1), \ldots, u(k-n+1)}{g[y(k), y(k-1), .., y(k-n+1), u(k-1), \ldots, u(k-n+1)]} \quad (7)$$

Which is realisable for $d \geq 2$. Figure 5 represents the block diagram of the NARMA-L2 controller.

The NARMA-L2 controller transforms a nonlinear plant into an approximately linear system using an explicit control law derived from an affine NN model of the plant's dynamics. This approach represents the output of a nonlinear system as the aggregation of two functions, $f[\cdot]$ and $g[\cdot]$, identified by neural networks, with all nonlinearities separated from the present control input (Richardson 2001; Skudder 1992; Stirling 1987; Uddin 2019).

The controller computes the subsequent control action by subtracting the predicted nonlinear system behaviour from the desired future output. Subsequently, it amplifies the outcome by the estimated input gain. This compensates for plant nonlinearities and produces approximately linear input–output behaviour in the closed loop, enabling precise reference tracking. The controller may operate in real time and avoids being trapped in algebraic loops, as the control input is computed one step ahead ($d \geq 2$). This characteristic makes the controller suitable for fast, nonlinear processes such as Ohmic heating systems.

Plant Identification of NARMA-L2 Controller

The experimentally collected CFOH input–output data were utilised to identify plants, a crucial stage in the development and testing of the controller. Accordingly, the input and output variables were established. The voltage supplied to the system served as the input variable, representing the thyristor setpoint. The output variable used was the final product temperature, designated as FT1, corresponding to the fibre optic temperature sensor readings at the outlet. The identification approach utilised data from the pilot-scale CFOH. This data was carefully selected to cover the entire range of CFOH operations. The resulting model effectively captures the temporal changes inside the system. This type of coverage is essential to ensure that the identified plant model is reliable and robust across different operational conditions. Figure 6 illustrates the process of plant identification by delineating the relationship between inputs and outputs and constructing a plant model.

To highlight the advantages of the proposed nonlinear modelling approach, it is useful to compare the NARMA-L2 model with conventional linear models, such as a first-order transfer function. For comparison, a conventional

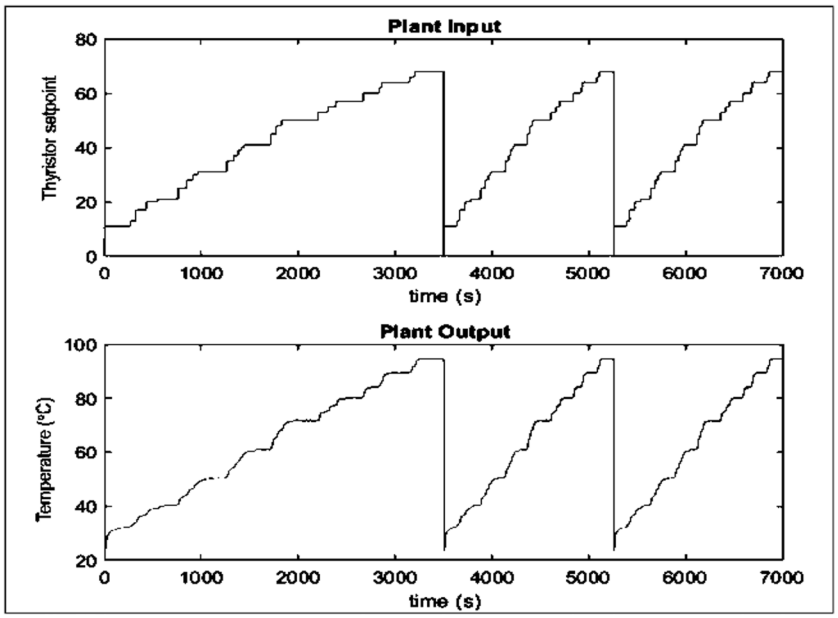

Fig. 6 Plant identification of NARMA-L2 controller

first-order linear thermal model can be expressed as follows:

$$G(s) = \frac{K}{\tau s + 1} \tag{8}$$

where K is the system gain and τ is the time constant. Such models assume linear system behaviour and are generally valid only around a specific operating point. In systems such as continuous-flow Ohmic heating, where electrical conductivity varies with temperature and strong coupling exists between electrical and thermal phenomena, the system dynamics are inherently nonlinear and time-varying. As a result, linear models may fail to accurately capture system behaviour across a wide operating range.

In contrast, the NARMA-L2 model represents the system as a nonlinear discrete-time mapping between past inputs and outputs and future outputs. This allows the model to capture complex nonlinear relationships directly from experimental data without requiring linearisation assumptions. Furthermore, the NARMA-L2 structure enables the derivation of an explicit nonlinear control law through feedback linearisation, allowing improved tracking performance and reduced overshoot in comparison to linear model–based controllers. Therefore, while linear models are simple and computationally efficient, the NARMA-L2 approach provides a more accurate and flexible representation of the CFOH system, particularly under varying operating conditions.

NARMA-L2 Neural Network Controller Training, Testing and Validation

The next phase involves training the neural network following plant identification. The neural-network models were trained using experimentally obtained input–output data from the pilot-scale CFOH system. The thyristor voltage (power setpoint) was used as the input variable, while the outlet temperature measured by the FT1 fibre optic sensor was used as the output variable. The data were sampled at 1 s intervals to adequately capture the dominant thermal dynamics of the process while maintaining computational efficiency.

The collected dataset was divided into training, validation and independent testing subsets using a 70:15:15 ratio. The training dataset was used to update the neural network weights, the validation dataset was used to monitor generalisation performance and prevent overfitting during training, and the testing dataset was reserved for independent evaluation of the final trained model. This data partitioning strategy is widely adopted in NN modelling, as it provides a balanced trade-off between model learning, overfitting control and unbiased performance assessment.

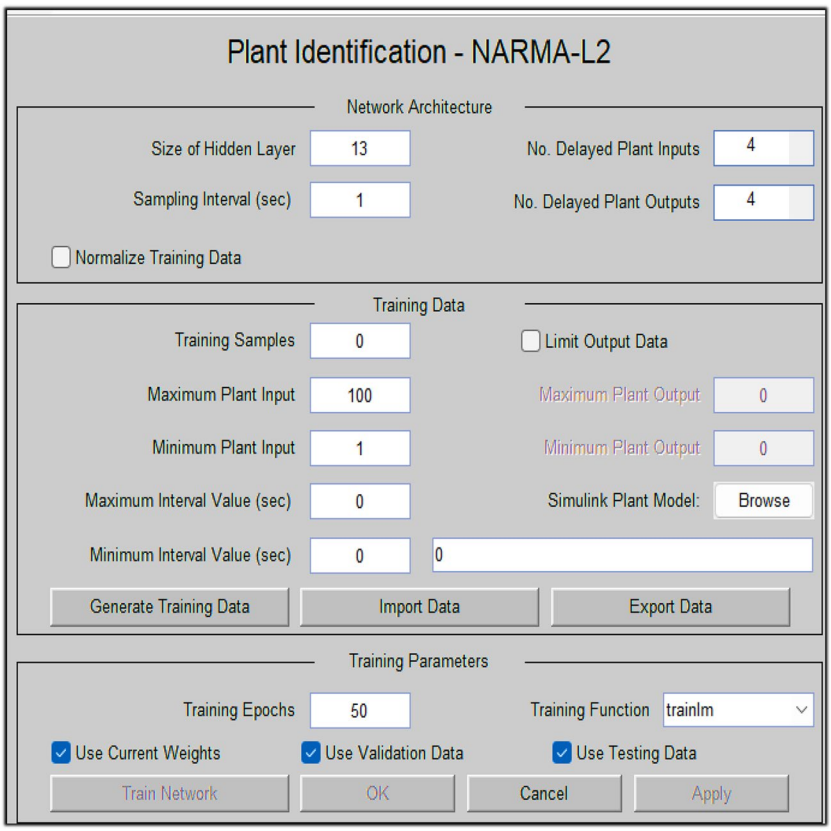

Fig. 7 NARMA-L2 controller training parameters

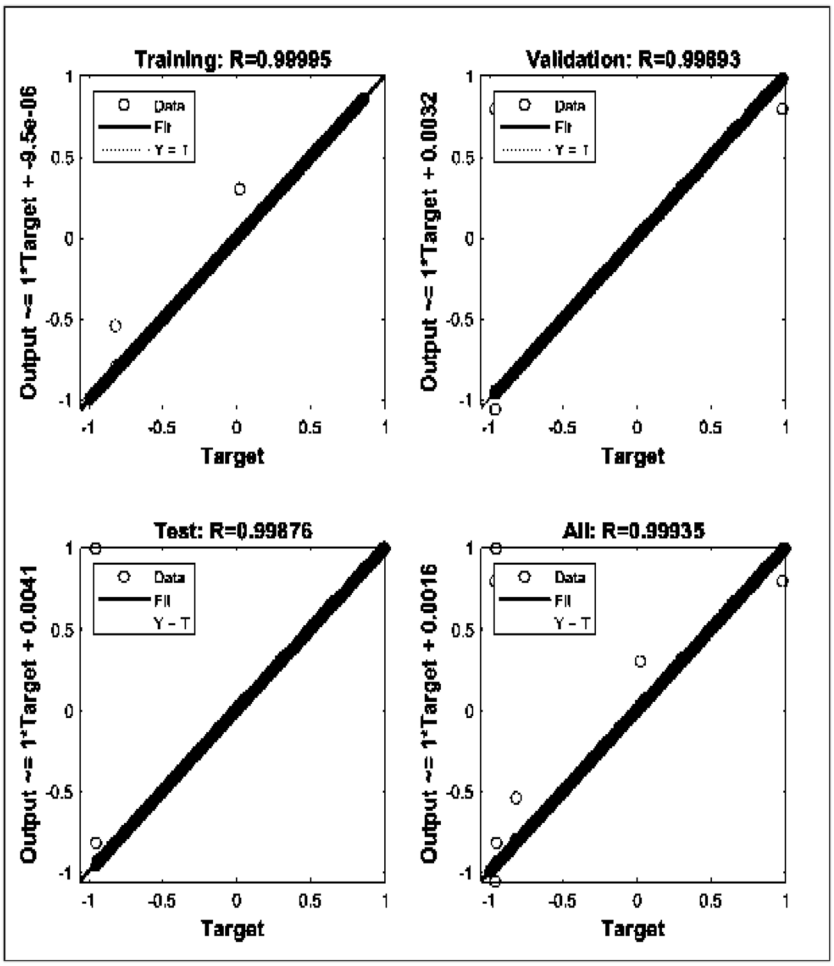

Fig. 8 NARMA-L2 regression plots

The NARMA-L2 neural-network hyperparameters were systematically selected to achieve accurate nonlinear prediction while maintaining computational efficiency, as illustrated in Fig. 7. The model was configured with a single hidden layer containing 13 neurons, along with four delayed inputs and four delayed outputs. The network was trained for 50 epochs using the Levenberg–Marquardt (LM) algorithm, which is well-suited for medium-sized networks due to its fast convergence and reliable performance.

These parameters were determined through systematic evaluation of different network configurations and delay combinations. The inclusion of four delayed inputs and outputs enables the model to effectively capture the dominant memory effects, thermal inertia and transport delay inherent in the CFOH process. A hidden layer size of 13 neurons was selected as it provided sufficient capacity to approximate the nonlinear plant dynamics, while avoiding unnecessary model complexity. Smaller networks resulted in reduced prediction accuracy, whereas larger networks did not yield significant improvements in validation performance.

Model performance was evaluated using regression analysis across the training, validation and testing datasets. The independent testing dataset was not used during the training process and was therefore utilised to assess the generalisation capability of the final trained model. Figure 8 illustrates the regression plots to evaluate the performance of the trained NARMA-L2 model across training, testing and validation phases. The corresponding regression values are 0.99995, 0.99876 and 0.99893. The overall regression value is 0.99935. These results indicate a strong correlation between neural network outputs and target values. Regression values close to 1 indicate a strong correlation between predicted and actual outputs.

Design of an NN-Based Model Reference Controller for Continuous Flow Ohmic Heater (CFOH)

MRC is a strategy in which the desired behaviour of a system is defined by a reference model, and the controller is designed to ensure that the actual plant output follows this reference model output. In essence, the controller

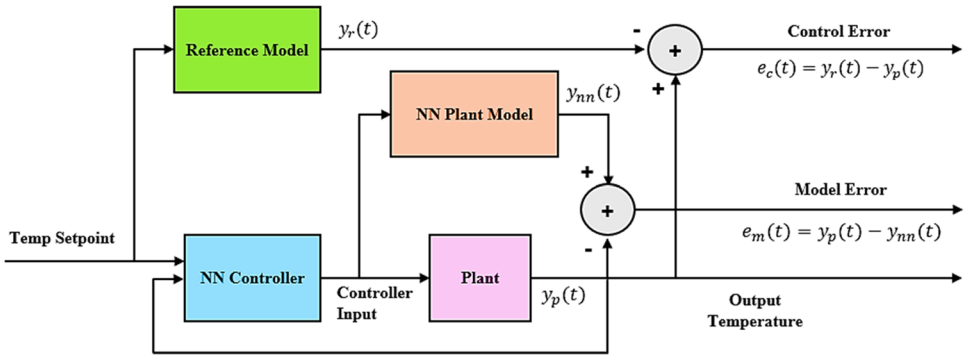

Fig. 9 Basic structure of model reference controller (MRC)

continuously adjusts the plant input to minimise the error between the plant output and the reference model output.

Figure 9 illustrates the structure of the MRC system, which consists of three main components: a neural network (NN) controller, an NN-identified CFOH plant model and a reference model. The NN-identified plant model represents the nonlinear dynamics of the continuous flow Ohmic heating system and is obtained from experimental input–output data. This model is primarily used during the controller training phase to simulate the plant behaviour and to enable controller optimisation without relying on continuous real-time experimentation. The NN controller is a separate neural network that generates the control input (thyristor setpoint) based on the reference signal, the measured plant output and past system behaviour. Its objective is to adjust the control input such that the plant output follows the desired response. The reference model defines the desired dynamic behaviour of the system, including characteristics such as response speed, stability and acceptable overshoot. It provides a target output trajectory that the actual plant output should track.

Although the NN-identified plant model captures the system dynamics, it does not specify the desired system performance. The reference model is therefore required to define the control objective. In the MRC framework, the controller is trained to minimise the error between the plant output and the reference model output. Thus, the plant model describes how the system behaves, while the reference model specifies how the system should behave. The NN controller learns to bridge this gap by generating appropriate control actions to achieve the desired performance.

In the proposed MRC architecture, the control input signal is simultaneously applied to both the reference model and the neural network controller. The reference model generates the desired output response, while the NN controller produces the control signal that is applied to the actual CFOH plant. The same control signal is also supplied to the NN plant model, which acts as an approximate representation of the real plant dynamics. The NN plant model is mainly used during controller training and optimisation to predict the plant response without requiring continuous experimentation on the physical system.

The actual plant output is continuously fed back to the NN controller, enabling the controller to adjust the control action according to the observed system behaviour. Within the MRC structure, two different error signals are utilised: the model error and the control error.

The model error represents the difference between the actual plant output and the output predicted by the NN plant model: where:$e_m(t)$= model error, $y_p(t)$= actual plant output and $y_{nn}(t)$= output predicted by the NN plant model.

This error is primarily used during the plant identification and training stage to improve the accuracy of the NN plant model. By minimising the model error, the neural network–based plant representation becomes a more accurate approximation of the real CFOH system dynamics.

The control error is defined as the difference between the desired reference model output and the actual plant output: where: $e_c(t)$ = control error, $y_r(t)$ = reference model output and $y_p(t)$= actual plant output.

The control error is the primary signal used by the NN controller during controller learning and optimisation. The controller adjusts its neural-network weights to minimise this error so that the actual plant output closely follows the desired response specified by the reference model.

Therefore, the model error is used to improve the accuracy of the NN plant model, whereas the control error is used by the NN controller to learn the appropriate control action required for accurate reference tracking and stable closed-loop operation. This dual-error structure enables the MRC framework to simultaneously achieve accurate plant modelling and effective control performance under nonlinear operating conditions.

In this architecture, the neural network controller has multiple inputs comprising delayed values of the reference input to account for reference changes over time, delayed values of the plant output and delayed values of its past control outputs. These delayed signals enable the controller to capture system memory and dynamic behaviour more effectively. The neural network plant model is usually a NARX-type

network (Nonlinear Autoregressive with Exogenous input) that takes inputs as the delayed control inputs (plant inputs) and delayed plant outputs, and outputs the predicted next plant output. This plant model network captures the plant's dynamics. The number of delay terms (past time steps) is chosen based on the system's order or memory.

In this context, it is important to clearly distinguish the role of the NARMA model from that of the MRC. Although both approaches utilise NN-based system representations, they are fundamentally different in structure and implementation. The NARMA-L2 model is used to directly derive a control law through feedback linearisation, where the nonlinear plant dynamics are explicitly cancelled to compute the control input. In contrast, the MRC framework does not directly invert the plant model. Instead, it employs a reference model that defines the desired system behaviour and trains a separate neural network controller to minimise the tracking error between the plant output and the reference model output. While a NARMA-type model can be used as the plant model within an MRC architecture, it cannot be directly used as a complete MRC controller, because MRC requires an additional learning process to determine the control action. Therefore, NARMA-L2 and MRC represent fundamentally different NN-based control methods: one based on direct nonlinear model inversion and the other based on reference-model tracking through adaptive controller learning.

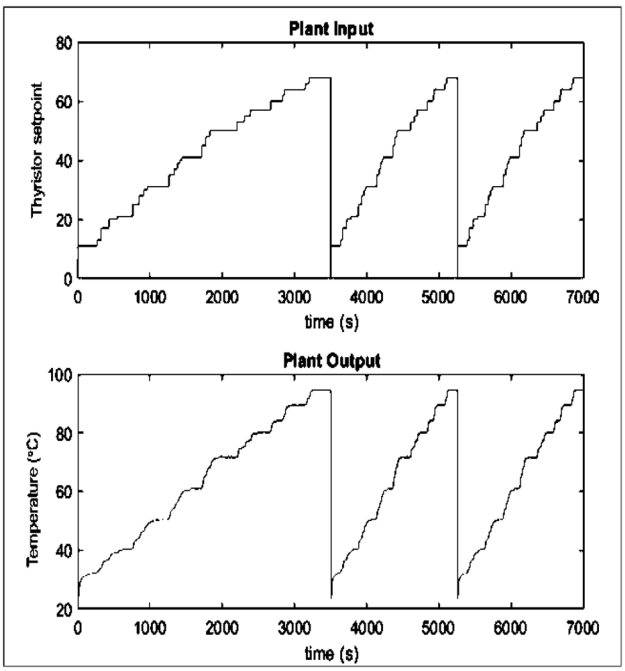

Fig. 10 Input–output data for plant identification

Plant Identification of Model Reference Controller

Before designing the controller, it is critical to obtain an accurate data-driven model of the plant. In this research, the plant identification was conducted using sweet and sour sauce as the product fluid, with an initial electrical conductivity of 0.6 S/m and a flow rate of 1 L/min (these conditions provide a consistent baseline for modelling). The input–output data for the plant identification process is shown in Fig. 10. The network architecture for this process was chosen using a grid search method, where the hyperparameters of the NARX network were tuned repeatedly until the target performance of the network model was achieved. The final architecture of the identified plant model is shown in Fig. 11.

The primary hyperparameters selected for the NARX-based plant identification mode are summarised below:

Network Architecture
Two-layer feedforward (NARX) network with 9 neurons in the hidden layer. A single hidden layer with 9 neurons was found sufficient to capture the plant's nonlinear behaviour without overfitting. This was empirically determined; 9 neurons gave good performance for the CFOH plant.
Delayed inputs/outputs
The network was configured with 2 delayed plant inputs and 2 delayed plant outputs. This means the plant model considers the last 2 time-step values of the input (thyristor setpoint) and output (temperature) when predicting the next output. The inclusion of two delayed inputs and outputs enables the network to capture dominant second-order thermal dynamics and transport-delay effects.

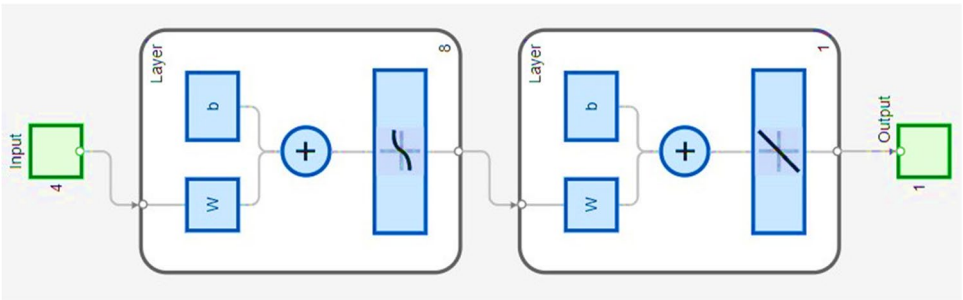

Fig. 11 Neural network architecture for plant identification

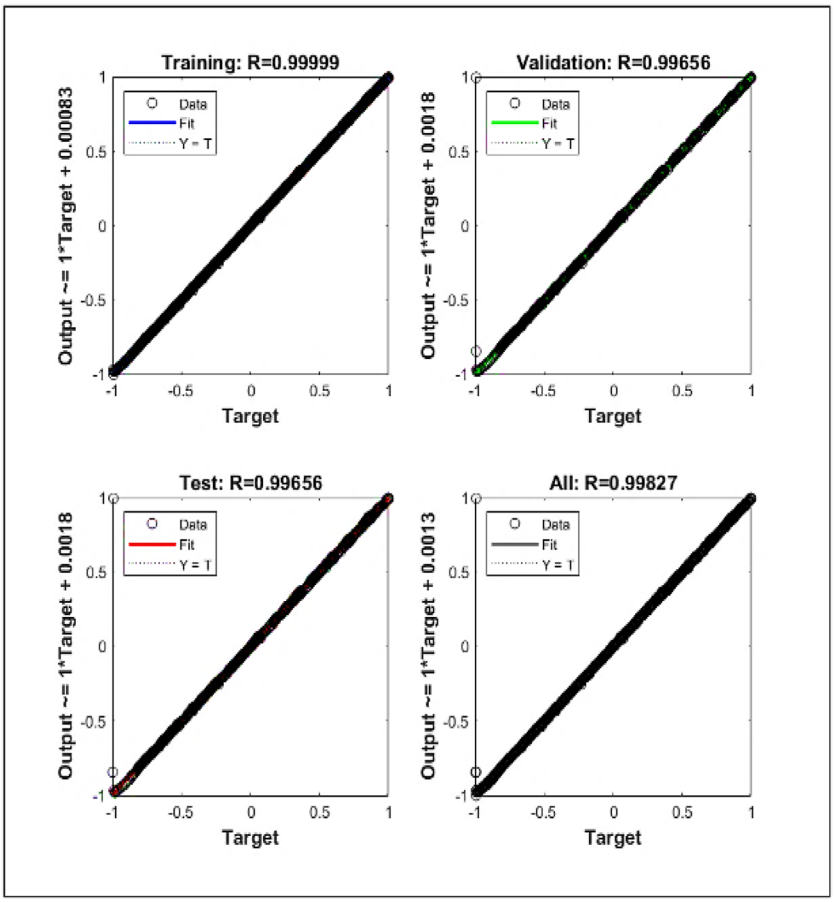

Fig. 12 Neural network architecture for plant identification

Sampling Interval

Data were sampled at 1-s intervals during the identification process. This sampling interval was selected to match the real-time data acquisition frequency of the pilot-scale CFOH system and was sufficiently short to capture the significant thermal dynamics of the process accurately.

Input Range

The plant input (thyristor power setpoint) was varied over a range of 1 to 100% during identification. This corresponds to the minimum and maximum CFOH power settings. The output temperature corresponding to this input range spanned roughly from the inlet

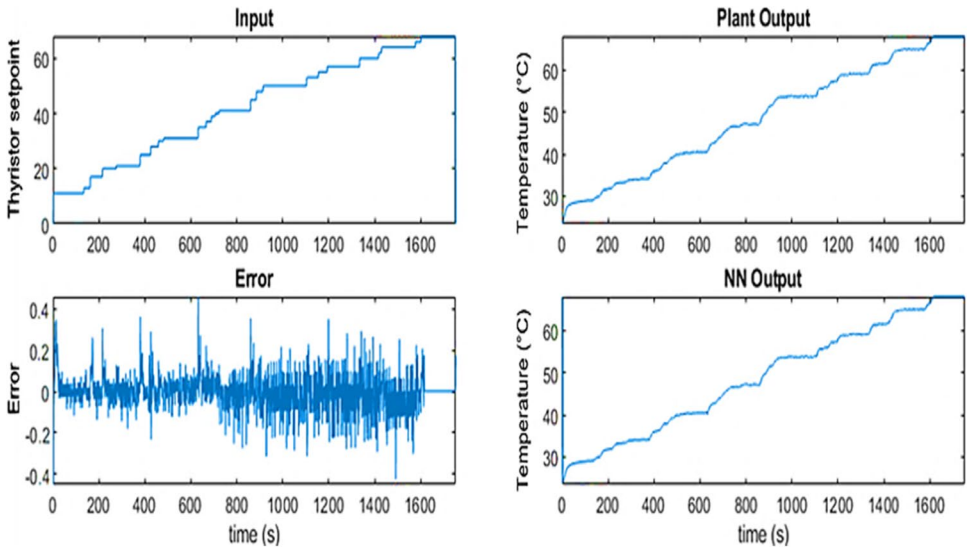

Fig. 13 Real-time plant output and NN-based plant identification output for test data

temperature (16 °C) up to near the maximum desired temperature (100° C).

Training Algorithm

Levenberg–Marquardt backpropagation (Trainlm) was used for training the neural network plant model. Trainlm is a fast, second-order optimisation method well-suited for moderate-sized networks, and it typically converges in relatively few epochs for function approximation tasks. In this design, 150 training epochs were chosen as an optimal balance between sufficient learning and the prevention of overfitting. Using trainlm, the network training converged to a mean squared error (MSE) of 0.0023 and an overall regression (R) value of 0.998 (as shown in Fig. 12), indicating that an accurate model of the plant was achieved.

The outcome of the plant identification was a neural network model that predicts the outlet temperature of the saline solution given the current and recent past values of the thyristor input and temperature. The accuracy of the model was validated by comparing its predictions to actual plant data not seen in training, shown in Fig. 13. As the CFOH process can be non-linear, the neural network approach is advantageous; it can capture these non-linear relationships where a simple linear model would falter. An accurate NN-based plant model is essential for reliable controller prediction, stable closed-loop operation and effective nonlinear control implementation within the defined operating region.

Model Reference Controller Training

After obtaining an accurate plant model, the next step was to design the MRC. The control goal is to make the outlet product temperature track a desired temperature trajectory, provided by the reference model, despite disturbances or nonlinearities. The design and training of the controller were also carried out in MATLAB/Simulink using the MRC block. The reference model used the state-space model defined in Eqs. 9 and 10.

$$x(k+1) = Ax(k) + B_u u(k) + B_v v(k) + B_d d(k)) \tag{9}$$

$$y(k) = Cx(k) + D_y v(k) + D_d d(k) \tag{10}$$

Where k is the time step index. In this model, $x \in \Re n$ is the state vector representing the system's temperature states, u is the control input (the voltage input to the Ohmic heater) and y is the controlled output (the product temperature). The terms v and d represent measured and unmeasured disturbances, respectively. For example, v could include mass flow rate or inlet temperature measurements if they were varying, while d might accumulate unmeasured effects like ambient losses or modelling error.

The matrices A,B_u,B_v,B_d, C, D_y and D_d define the dynamic relationships between these variables. This state-space formulation can accommodate time-varying parameters; however, a conventional MPC assumes these matrices remain fixed around a nominal operating point, implying that it is a linearised steady-state model. For the CFOH system in this research, a linearised state-space model was obtained around the normal operating conditions. The model has two states ($x = 2$), which capture the thermal dynamics of the continuous flow Ohmic heater. The specific state matrices at the nominal point are given below.

$$A = \begin{bmatrix} 0.997 & 0.296 \\ -7.19 \times 10^{-4} & 0.969 \end{bmatrix} \tag{11}$$

$$B_u = \begin{bmatrix} 8.3 \times 10^{-5} \\ 5.5 \times 10^{-4} \end{bmatrix} \tag{12}$$

$$C = \begin{bmatrix} h & i \\ 1 & 0 \end{bmatrix} \tag{13}$$

The state matrix A indicates that the first state (product temperature) tends to persist with a factor of 0.997 each step (very slow decay, effectively near integrator), and it is coupled to the second state with the 0.296 term. The second state (representing thermal accumulation in the heating chamber) also has a high factor of 0.970 and a small coupling back to the first state, -7.19×10^{-4}. Overall, the eigenvalues of A are close to 1, reflecting the slow dynamics and strong thermal inertia of the system.

The input matrix B_u represents changes in the manipulated variable (voltage input), $u(k)$, that have a direct, though small, effect on both states. Notably, the second state has a larger gain (5.5×10^{-4}) from the input than the first state (8.3×10^{-5}), suggesting the input initially influences an internal energy state which then drives the output state. For this model, we did not include any measured disturbance inputs, so $B_v = 0$.

Likewise, there were no direct unmeasured disturbance influences on the state equation, so $B_d = 0$. The output matrix C means the controlled output y is taken to be the first state directly. In this case, that first state corresponds to the outlet fluid temperature. The second state is not directly measured as an output, but it influences the first state through the dynamics in matrix A. The contribution of the second state to the first output is weighted by i. The terms $D_y = 0$ and $D_d = 3.3 \times 10^{-4}$ have no direct feedthrough from any measured disturbance to the output. However, a small constant term $D_d = 3.3 \times 10^{-4}$ provides a bias on the output from unmeasured disturbances. The value is very small; it can account for a slight offset in temperature that is captured by the states. This helps the controllers to eliminate steady-state error by accounting for the fact that a tiny constant input might be needed to maintain temperature (for example, compensating for heat losses).

The NN controller is a two-layer network (one hidden layer) with the following configuration.

Hidden Layer Size

The number of hidden neurons in the MRC controller network was determined through incremental tuning and performance evaluation. The controller must learn a more complex mapping compared to the plant model, as it relates reference inputs, plant outputs and past control actions to the required control signal. Therefore, a larger network capacity was necessary. Several configurations were evaluated, and the number of neurons was increased until improvements in tracking performance and convergence stabilised. A hidden layer size of 35 neurons was selected as it provided accurate reference tracking, reduced steady-state error and stable training behaviour. Further increases in neuron count did not produce meaningful improvements in tracking accuracy, while significantly increasing computational complexity.

Controller Inputs (Delays)

The controller was provided with two delayed reference inputs, two delayed plant outputs and two delayed controller outputs. In total, that means at each time step the controller sees the current reference $r(t)$ and one past value $r(t-\Delta t)$; the last two measurements of the plant output (temperature) $y(t)$, $y(t-\Delta t)$ and the last two control signals, it generated $u(t-\Delta t)$, $u(t-2\Delta t)$. Here, Δt represents the sampling interval of the discrete-time system. These inputs give the controller's memory of what has recently happened. Including delayed plant outputs helps the controller account for the plant's inertia and trend (e.g., is temperature rising or falling), and including delayed controller outputs (past actions) helps it understand how its previous actions are still affecting the plant (since the plant has memory). The two delayed reference inputs allow the controller to anticipate changes; if the reference is going to or has just changed, the controller can begin to respond proactively. This structure (with multiple delays) is a standard design in model reference neural controllers.

Controller Output

The output of the controller network is the manipulated variable for the plant, in the case of this research, the thyristor setpoint. The controller's task is to output the correct power level $u(t)$ such that the plant's temperature reaches the desired value. The controller output was constrained within the allowable actuator range of 1–100%

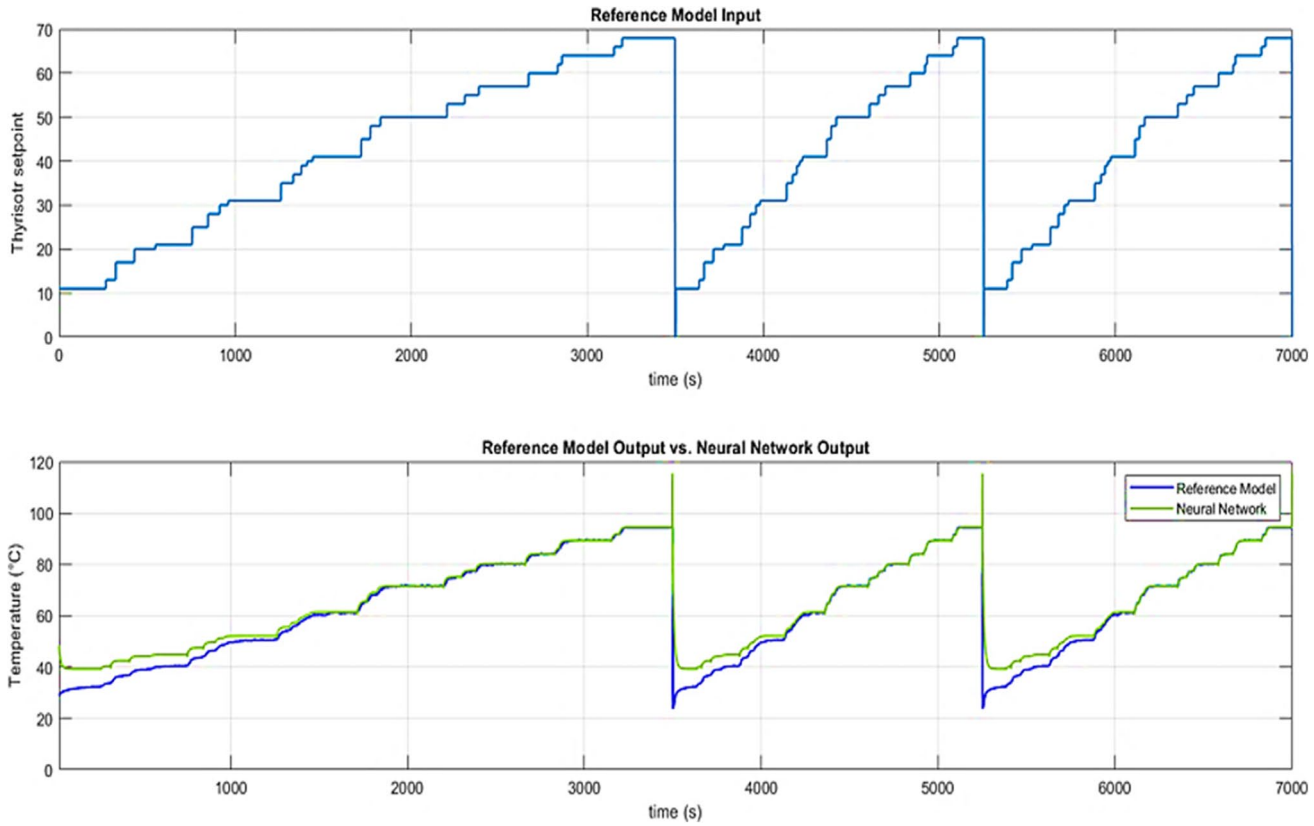

Fig. 14 MRC plant model vs. neural network outputs

Training Method

The controller network is trained with the plant model in the loop using dynamic backpropagation across time. A sequence of reference inputs is generated, the closed-loop simulation with the plant model is executed to obtain the plant output, the error relative to the reference model output is computed, and subsequently, the controller weights are adjusted to minimise this error. This process effectively requires backpropagating the error through the plant model and controller over time since the controller's current action affects future errors. The controller network was trained for 120 epochs to provide sufficient weight convergence without overfitting. It is noteworthy that the time required for each controller training cycle is almost twice that of plant model training, due to the need for dynamic backpropagation through sequences. Each training iteration must simulate the identified plant dynamics forward in time and propagate errors backwards through time, which is computationally intensive.

After completing the training process, the NN controller was configured with the final optimised weights. To assess its performance, the NN output was compared against the corresponding output of the plant model (the results are displayed in Fig. 14). This comparison confirmed that the controller was capable of accurately tracking the reference model.

Implementation of the Developed Controllers in the MATLAB/Simulink Environment CFOH Physical Model

Employing a validated physical model provides a safe, adaptable and energy-efficient method for testing controllers while maintaining a close approximation to the actual process. A physical model (often implemented in a simulation environment) aims to represent the actual system's behaviour more realistically by incorporating coupled multiphysics interactions.

Unlike a highly simplified transfer function, a physical model can include nonlinear relationships and directly utilise physical laws, resulting in improved accuracy. Physical models are better at capturing complex and dynamic behaviours, such as the coupling between electrical and thermal fields and the feedback of temperature on electrical conductivity, which are difficult to represent using simplified linear models.

Additionally, a physical model can be interfaced with real-time data: sensor measurements from the operating system are fed into the model to update its states, effectively creating a digital twin of the process. This capability enables advanced applications like predictive monitoring, fault detection and model-based control, where the model runs in parallel with the actual process and assists in adjusting control inputs. In this study, a high-fidelity, real time–validated physical model of CFOH is used to test the developed control strategies and optimise performance without risking actual product or equipment (Vandoren 1998).

Results and Discussion: Comparative Performance Analysis of the Controllers

Setpoint Tracking

NARMA-L2, MRC and PID controllers were implemented in MATLAB/Simulink simulation using the real time–validated CFOH plant model developed and published in (Vandoren 1998). The simulation was based on a proprietary

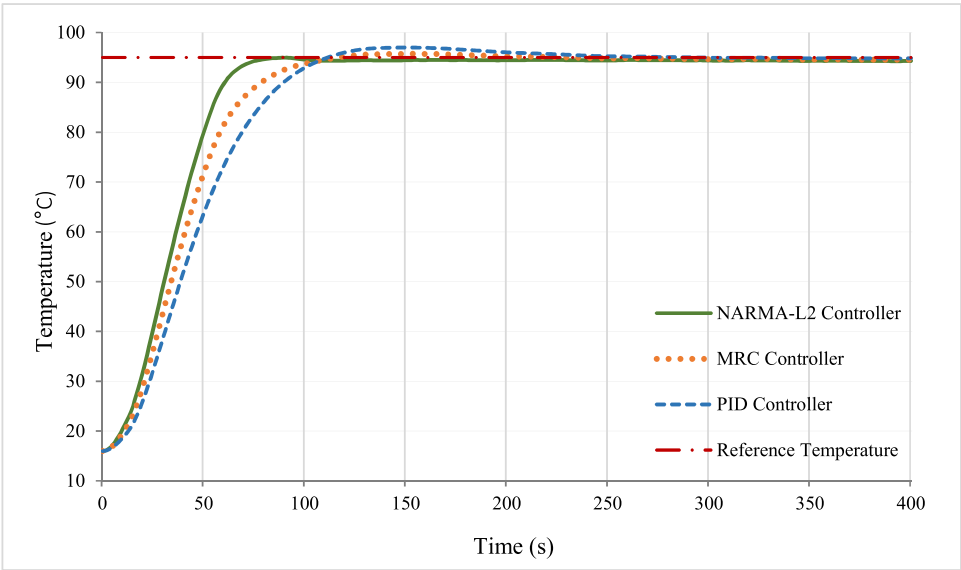

Fig. 15 Simulated temperature responses of NARMA-L2, MRC and PID controllers during heating of sweet and sour sauce from 16 to 95 °C at an initial electrical conductivity of 0.60 S/m

sweet and sour sauce obtained from a local industry, ensuring realistic operating conditions. The product entered the system at an initial temperature of 16 °C with an electrical conductivity of 0.60 S/m. Each controller was designed to regulate the heating process and achieve a target outlet temperature of 95 °C, representing a typical pasteurisation condition. The controllers were evaluated under identical operating conditions to enable a fair comparison of their dynamic performance, including rise time, settling time and stability. Figure15 illustrates the temperature response of each controller, highlighting their ability to track the desired setpoint and maintain process consistency within the CFOH system.

Performance Metrics

The effectiveness of the designed controllers in sustaining the target temperature of 95° C is assessed using several performance metrics. The comparative dynamic performance analysis demonstrates that NN-based controllers exhibit improved performance over classical PID controllers across all transient response metrics. The NARMA-L2 controller exhibits a rise time of merely 54.76 s, which is approximately 17.8% faster than the MRC (66.58 s) and 30.4% faster than the PID controller (78.64 s), as illustrated in Table 1. This demonstrates the high responsiveness of the NARMA-L2 controller. The reduced rise time enables it to rapidly achieve the desired temperature more effectively than other controllers.

Transient time, representing the duration required for the system to recover and stabilise following a significant change, was shortest for the NARMA-L2 controller at 69.74 s. The MRC controller required 96.51 s, whereas the PID controller necessitated 177.95 s. The shorter transient phase indicates that the NARMA-L2 and MRC controllers are more effective in mitigating prolonged oscillatory behaviour and accelerating the transition to steady-state operation. The settling time further illustrates the efficacy of advanced control strategies. The settling time, which indicates the time required for the system's response to remain within a specified tolerance band around the setpoint, was significantly decreased under NARMA-L2 control, achieving steady-state conditions in 68.31 s. The MRC required 93.69 s, whilst the PID controller took far longer, at 163.23 s, to stabilise. This demonstrates that the NARMA-L2 and MRC enhance convergence speed and improve closed-loop stability.

The NARMA-L2 controller demonstrated improved performance regarding overshoot by maintaining the system output within the specified temperature limits. The MRC experienced a slight overshoot of 0.78%, whereas the PID controller exhibited a more substantial overshoot of 2.10%. None of the controllers induced undershoots, which is significant, as it indicates that the system response did not fall below the setpoint during transient operation. The NARMA-L2 controller exhibits improved dynamic performance under the simulated conditions, characterised by a more rapid reaction, reduced oscillations and enhanced stability. This renders it particularly effective for accurate and energy-efficient temperature regulation in CFOH. The MRC controller exhibits moderate performance with an acceptable overshoot. The PID controller shows comparatively inferior performance regarding responsiveness and overshoot characteristics.

Energy Efficiency and Power Consumption Analysis

The comparative examination of the NARMA-L2, MRC and PID controllers during the simulation period reveals significant differences in both the transient (1–70 s) and steady-state (71–400 s) phases, as illustrated in Table 2. The initial delay of around 15 s in the power and efficiency profiles is primarily attributed to inherent process dynamics, including thermal inertia, temperature-dependent electrical conductivity and fluid residence time. Minor contributions arise from sensor latency and controller initialisation. The subsequent rapid rise in power results from the nonlinear enhancement of electrical conductivity and the efficient utilisation of the controller.

During the transient phase, NARMA-L2 exhibits the highest average power consumption at 6043.58 W, followed by MRC at 5508.40 W and PID at 4973.23 W. Thus, the energy consumption during this period is highest for NARMA-L2

Table 1 Performance analysis of NARMA-L2, MRC and PID controllers for sweet and sour sauce heating from 16 to 95 °C with 0.6 S/m conductivity

Performance metric	NARMA-L2 controller	MRC controller	PID controller	Improvement of NARMA-L2 vs. PID (%)	Improvement of MRC vs. PID (%)
Rise time (s)	54.76	66.58	78.64	30.36	15.34
Transient time (s)	69.74	96.51	177.95	60.81	45.77
Settling time (s)	68.31	93.69	163.23	58.15	42.60
Overshoot (%)	0.00	0.78	2.10	100	62.86
Undershoot (%)	0.00	0.00	0.00	-	-

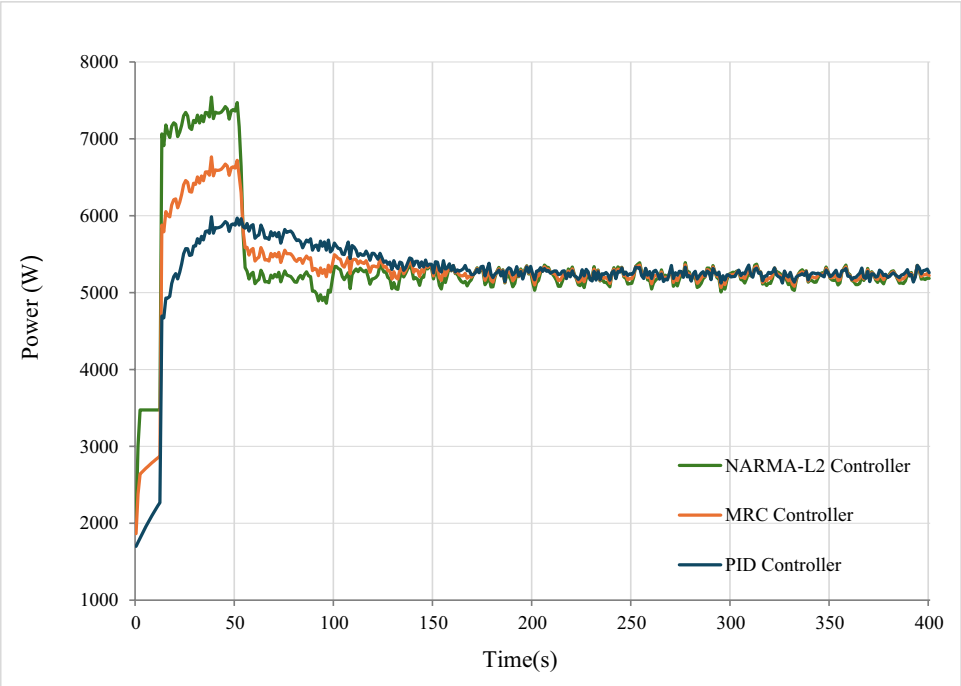

Fig. 16 Comparison of power consumption profiles of NARMA-L2, MRC and PID controllers during heating of sweet and sour sauce from 16 to 95 °C at an electrical conductivity of 0.60 S/m

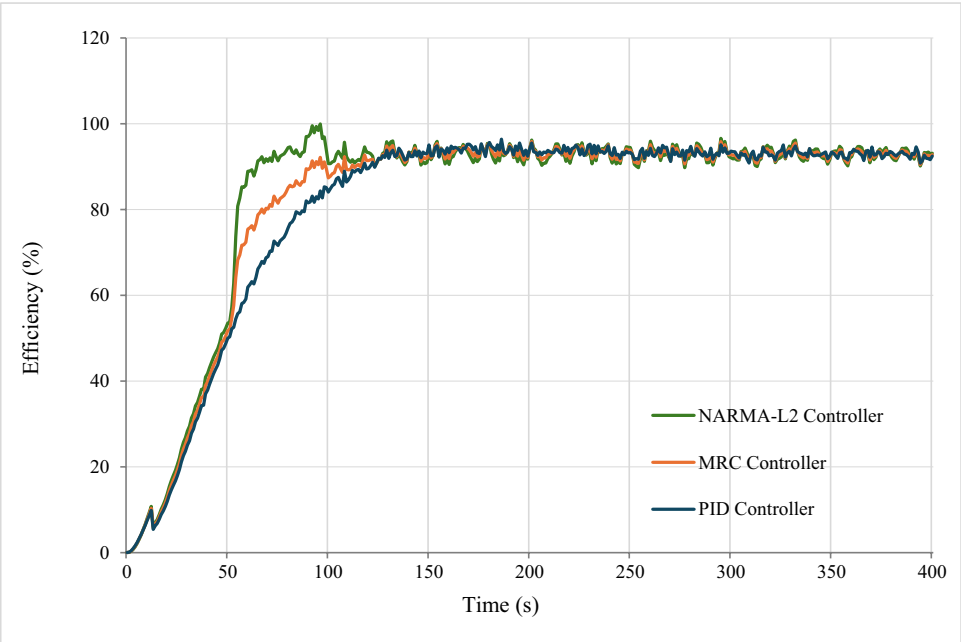

Fig. 17 Comparison of energy efficiency achieved by NARMA-L2, MRC and PID controllers during heating of sweet and sour sauce from 16 to 95 °C at an electrical conductivity of 0.60 S/m

Table 2 Comparison of power consumption and energy efficiency of NARMA-L2, MRC and PID controllers during heating of sweet and sour sauce from 16 to 95 °C at an electrical conductivity of 0.60 S/m

Controller	Average power (W)		Energy (kWh)		Efficiency (%)	
	1–70 s	71–400 s	1–70 s	71–400 s	1–70 s	71–400 s
NARMA-L2	6043.58	5202.39	0.1191	0.4769	35.37	92.99
MRC	5508.40	5259.88	0.1086	0.4822	36.21	92.28
PID	4973.23	5317.37	0.0980	0.4874	29.04	91.55

(0.1191 kWh), indicating a more aggressive response to initial system changes. In contrast, the PID controller, while showing the lowest energy consumption in this phase (0.0980 kWh), also reveals the lowest efficiency (29.04%), indicating lower effectiveness in converting input energy into useful control action during the transient period. The.

MRC demonstrates a balance between moderate energy consumption (0.1086 kWh) and relatively high efficiency (36.21%), highlighting its capacity to efficiently regulate system dynamics while maintaining optimal energy utilisation. The power consumption and energy efficiency profiles are shown in Figs. 16 and 17.

In the steady-state phase (71–400 s), all controllers achieve similar average power levels, with PID (5317.37 W) slightly surpassing MRC (5259.88 W) and NARMA-L2 (5202.39 W). Regarding the energy consumption, PID consumes 0.4874 kWh, marginally higher than MRC (0.4822 kWh) and NARMA-L2 (0.4769 kWh). Despite slight fluctuations in power, the efficiencies of all controllers remain high, exceeding 91%, indicating effective energy utilisation during steady-state operation. NARMA-L2 exhibits the highest efficiency (92.996%) in this phase, signifying a strong ability to maintain system operation with minimal energy consumption.

This result demonstrates that the selection of a controller should consider the trade-off between long-term energy efficiency and transient response speed. NARMA-L2 is the superior choice for steady-state efficiency and faster response, while MRC is an excellent option for overall balanced performance and robust control characteristics, as illustrated in Fig. 18.

Robustness Analysis of the Controllers

In addition to the above pasteurisation scenarios, robustness tests were also conducted in simulation for all three controllers. The CFOH model was subjected to a range of simulated disturbances, including variations in initial electrical conductivity, flow rate, inlet temperature, measurement noise and step changes in setpoint, to provide a more comprehensive assessment of controller performance.

Controller Performance Under Different Initial Electrical Conductivity

The electrical conductivity of real food products can vary between batches or over the course of heating. To simulate variation that may occur in real food processing conditions, the model was subjected to.

scenarios where the initial conductivity of the sauce was varied from 0.60 S/m, i.e., a low-conductivity case at 0.50 S/m and a high-conductivity case at 0.70 S/m, representing about ± 16.7% variation. The controllers were not retuned for these cases, thereby testing their robustness to modelling uncertainties. In the robustness evaluation, all three controllers (NARMA-L2, MRC and PID) maintained similar temperature response

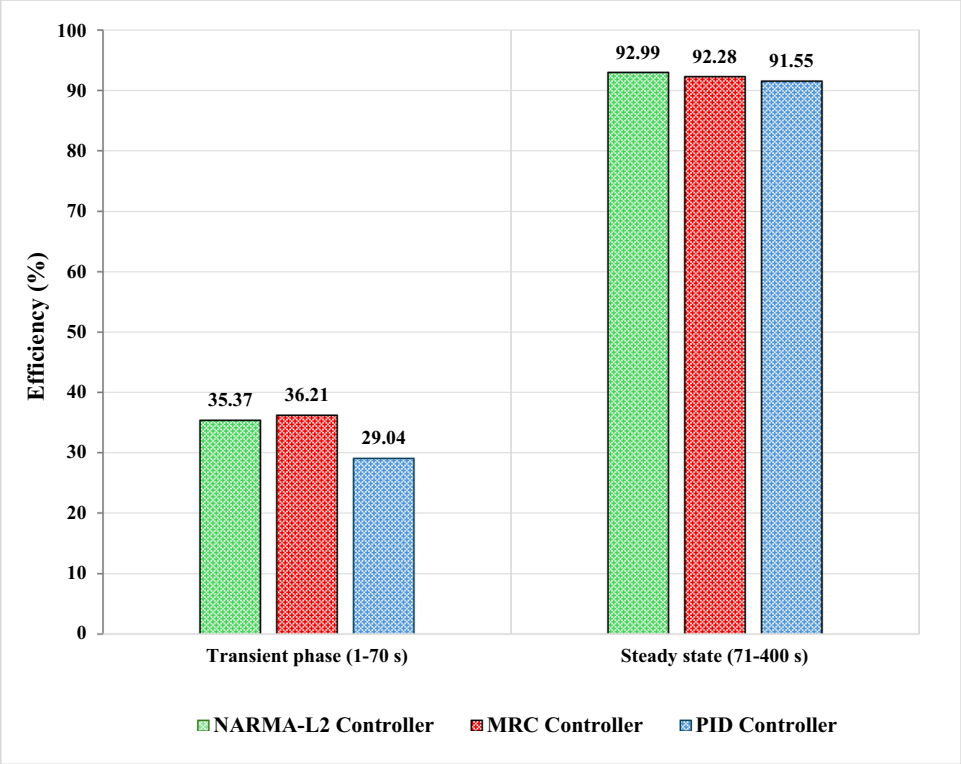

Fig. 18 Comparison of transient and steady-state energy efficiency of NARMA-L2, MRC, and PID controllers during heating of sweet and sour sauce from 16 to 95 °C at an electrical conductivity of 0.60 S/m

characteristics, as shown in Figs. 19 and 20. The transient response (e.g., rise and settling times) remained largely consistent across these conductivity values, with a maximum variation of approximately 2–3 s in settling time relative to the 0.60 S/m case. This indicates that each controller effectively handled the change in conductivity without significant performance degradation, which indicates robust controller performance.

Flow Rate Variation Analysis

To evaluate controller robustness under varying process conditions, simulations were conducted at two flow rates: a low flow rate of 0.5 L/min and a high flow rate of 1.5 L/min relative to the nominal operating condition. Variations in flow rate can significantly influence heat transfer characteristics and

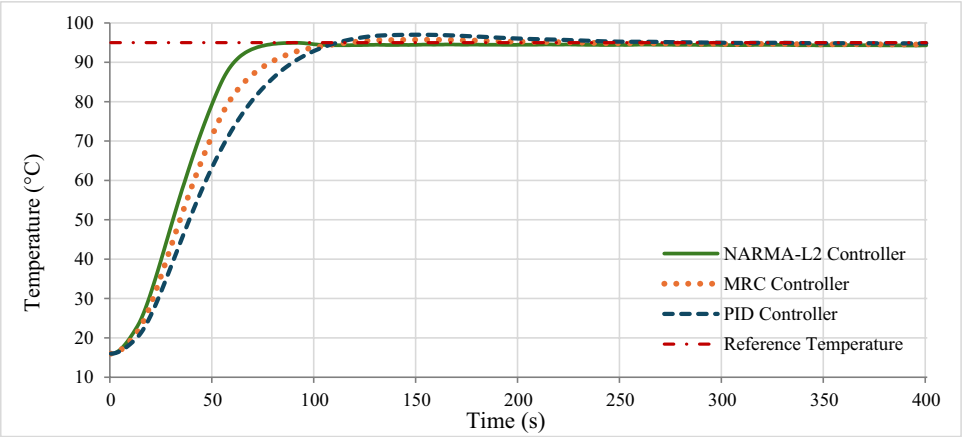

Fig. 19 Simulated temperature responses of NARMA-L2, MRC and PID controllers for sweet and sour sauce under low initial electrical conductivity conditions ($\sigma = 0.50$ S/m)

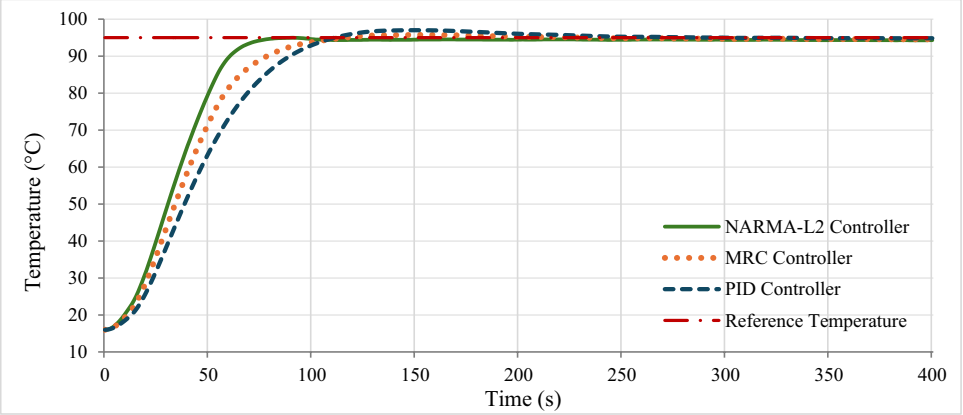

Fig. 20 Simulated temperature responses of NARMA-L2, MRC and PID controllers for sweet and sour sauce under high initial electrical conductivity conditions ($\sigma = 0.70$ S/m)

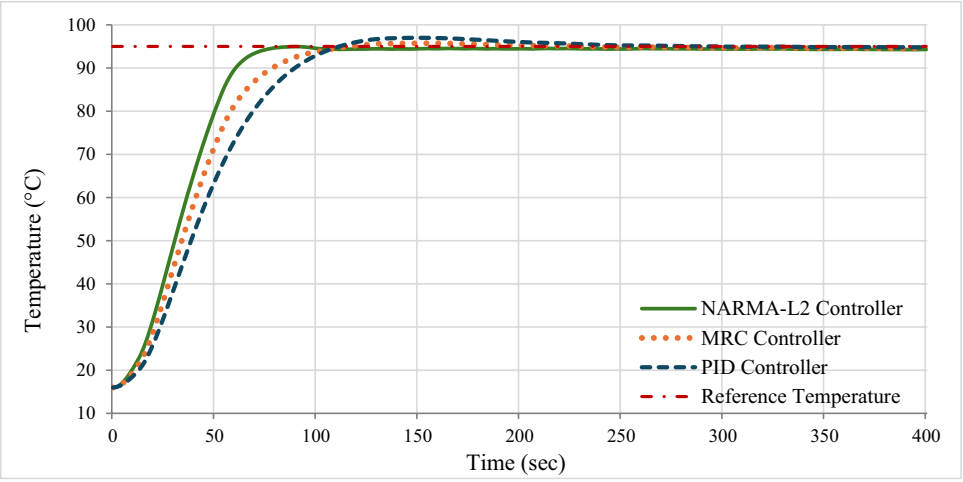

Fig. 21 Simulated temperature responses of NARMA-L2, MRC and PID controllers for sweet and sour sauce at a flow rate of 0.50 L/min

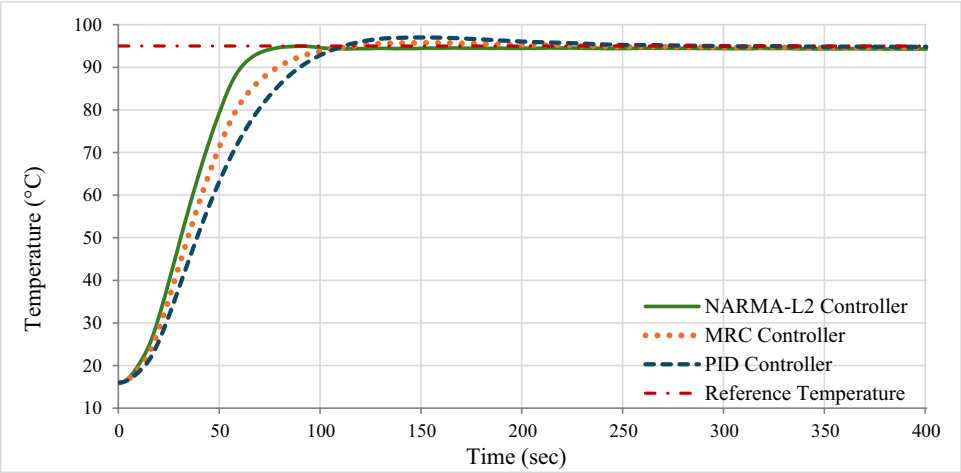

Fig. 22 Simulated temperature responses of NARMA-L2, MRC and PID controllers for sweet and sour sauce at a flow rate of 1.50 L/min

residence time within the CFOH system, thereby affecting temperature control performance. In this study, the controllers (NARMA-L2, MRC and PID) were not retuned, allowing assessment of their adaptability to such changes.

As illustrated in Figs. 21 and 22, all three controllers demonstrated stable and consistent temperature responses under both flow conditions. While slight variations in rise time and settling time were observed due to changes in residence time, the overall control performance remained satisfactory. The NARMA-L2 controller showed slightly faster adaptation, whereas MRC and PID maintained comparable stability. These results indicate that all controllers effectively handled flow rate variations without significant degradation in performance, confirming their robustness under dynamic processing conditions.

Inlet Temperature Disturbance

Robustness to inlet temperature variations was evaluated by increasing the inlet temperature from 16 to 21 °C while keeping the controller parameters unchanged. As shown in Fig. 23, all three controllers (NARMA-L2, MRC and PID) maintained stable temperature responses. Minor variations in rise and settling times were observed due to reduced heating demand; however, overall performance remained consistent, demonstrating effective disturbance rejection and robustness to inlet temperature changes.

Sensor Noise Analysis

To evaluate robustness against measurement uncertainty, Gaussian sensor noise with a variance corresponding to 0.5 °C was added to the temperature signal. As shown in Fig. 24, all three controllers (NARMA-L2, MRC and PID) maintained stable operation despite the noisy measurements. Minor fluctuations were observed in the control response, but tracking performance remained satisfactory, demonstrating the controllers' ability to handle sensor noise effectively without significant degradation.

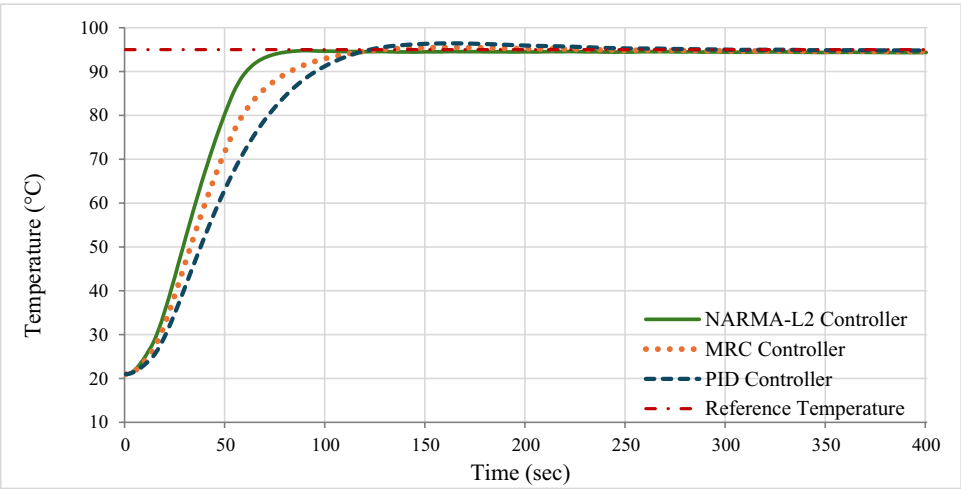

Fig. 23 Simulated temperature responses of NARMA-L2, MRC and PID controllers for sweet and sour sauce with an inlet temperature of 21 °C

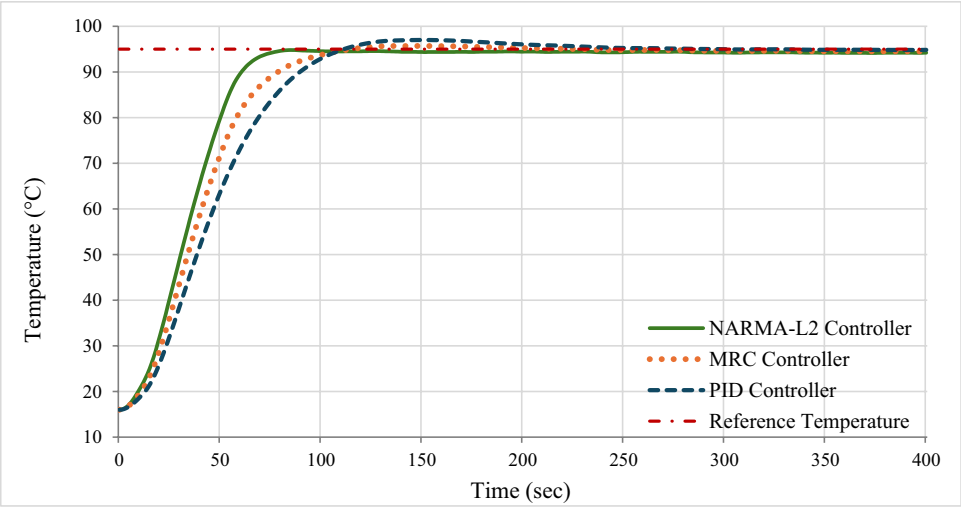

Fig. 24 Simulated temperature responses of NARMA-L2, MRC and PID controllers for sweet and sour sauce under sensor noise conditions ($\sigma = 0.5$ °C)

Controller Robustness Under Varying Setpoint Conditions

Another important robustness test for control systems involves assessing their response to sudden setpoint changes, which directly challenge the ability of the controller to handle large disturbances while maintaining stability, accuracy and efficiency. In the context of continuous flow Ohmic heating, where temperature must be precisely regulated in the presence of unpredictable input fluctuations such as food composition, flow rate, or desired product profile, the ability to adapt rapidly to such changes becomes essential.

To evaluate this, a step change in the reference temperature was introduced, which was from an initial steady state of approximately 50 °C to a final setpoint of 95 °C at 250 s into the test sequence. The resulting temperature responses under NARMA-L2, MRC and PID controllers are presented in Fig. 25. The results reveal that all three controllers accurately tracked the change in temperature setpoints. The NARMA-L2 controller reaches the setpoint fastest, followed by the MRC and PID controllers. These results demonstrate that NN-based controllers are more resilient and responsive than PID control.

Generalisation Across Process Variations

The robustness analysis demonstrates that the trained NN-based controllers maintain stable and consistent performance under variations in electrical conductivity, flow rate, inlet temperature, step change in setpoint and sensor noise. These results indicate that the neural network model can generalise beyond the specific training conditions to a reasonable

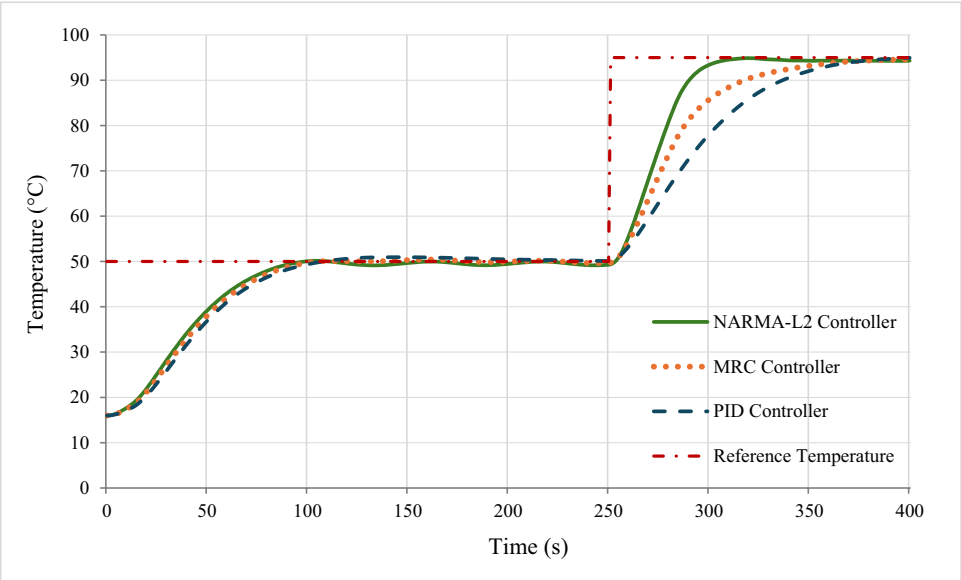

Fig. 25 Simulated temperature responses of NARMA-L2, MRC and PID controllers for a step change in setpoint temperature from 50 to 95 °C at an initial electrical conductivity of 0.60 S/m

extent. This generalisation capability arises from the ability of neural networks to approximate nonlinear input–output relationships over a range of operating conditions when trained on representative data.

Variations in electrical conductivity, which serve as a proxy for changes in food properties, showed minimal impact on control performance, suggesting that the model captures the dominant thermal–

electrical dynamics of the CFOH system. Similarly, changes in flow rate and inlet temperature resulted in only minor variations in dynamic response, while the system remained stable under measurement noise.

However, it should be noted that the model was trained using a specific food product and a defined operating range. For significantly different food types with substantially altered thermophysical properties or for extreme deviations in operating conditions, the prediction accuracy of the model may degrade. In such cases, retraining or updating the neural network with new input–output data would be required to ensure reliable performance. This is a common characteristic of data-driven models and represents an important consideration for practical deployment in diverse industrial applications.

Discussion on Sustainability Impacts

The carbon emission efficiency of the NARMA-L2, MRC and PID controllers was evaluated based on their steady-state energy consumption during the 71–400 s operational period of the CFOH system. The emissions analysis presented in this study is based on simplified assumptions, including fixed UK electricity emission conversion factors for 2025 (Zhang 2022) and steady-state energy consumption derived from simulation results. This analysis provides an indicative estimation of indirect emissions and does not constitute a full life cycle assessment. The emission conversion factors represent GHG emissions per kWh of energy consumed, indicating a total emission intensity of 0.177 CO_2e kg/kWh, which includes 0.17489 kg CO_2/kWh, 0.00090 CH_4 kg/kWh and 0.00122 N_2O kg/kWh.

Assuming the system operates continuously, the energy consumption per steady-state cycle was extrapolated to yearly utilisation. Under the stated assumptions, the results indicate that the NARMA-L2 controller consistently exhibits the lowest emissions across all parameters. The MRC follows; however, the PID controller exhibits the highest emissions. This trend is a direct consequence of the controllers' comparative energy efficiency. A decrease in steady-state energy demand results in a reduction of carbon intensity. The NARMA-L2-based controller emits approximately 8083 kilos of CO_2e annually. The MRC emits 8176 kg of CO_2e, whereas the PID controller emits 8270 kg of CO_2e, as seen in Table 3. Although the differences in energy usage each cycle are negligible, prolonged operation of the machine significantly affects long-term greenhouse gas emissions.

The PID controller generates approximately 184 kg more CO_2 annually compared to the NARMA-L2 controller. Similarly, emissions of CH_4 and N_2O remain small in absolute terms but contribute to the total CO_2-equivalent footprint. These findings demonstrate that sophisticated neural network-based controllers not only enhance control performance but also offer tangible environmental benefits through improved energy efficiency. To contextualise these results against conventional liquefied petroleum gas (LPG) heating methods. The heat transfer equation $Q = \dot{m} \cdot C_P \cdot \Delta T$ is used to calculate the energy required to elevate the temperature using LPG heating. where q represents the heat duty in kW, $\dot{m}$ denotes the mass flow rate of the sauce (0.01767 kg/s, approximately 1 L/min), C_P denotes the specific heat capacity of the sauce (3.8 kJ/kg·°C) and ΔT indicates the temperature increase from 16 °C to 95 °C. The sauce absorbs a net thermal energy of E=0.4847 kWh during the steady-state window. Considering that industrial gas heating operates at approximately 75% efficiency (Zhang & Wang 2023), the required amount of LPG energy each cycle increases to 0.6463 kWh. Utilising UK emission figures for LPG (CO_2: 0.23032 kg/kWh, CH_4: 0.00020 kg/kWh, N_2O: 0.00012 kg/kWh) (Zhang 2022), the emissions per cycle amount to 0.1487 kg CO_2e. This totals 39.08 kg each day and 14,270 kg per year when the system operates continuously. Based on the simplified assumptions used in this analysis, LPG heating is estimated to result in higher emissions compared to the CFOH system; however, these values should be interpreted as indicative rather than definitive. These findings highlight the importance of integrating high-efficiency

Table 3 Comparison of greenhouse gas (GHG) emissions for NARMA-L2, MRC and PID controller-based CFOH heating and conventional LPG heating using the UK 2025 electricity emission conversion coefficients

Controller	N_2O (kg/year)	CH_4 (kg/year)	CO_2 (kg/year)	Total CO_2e (kg/year)
NARMA-L2 (Ohmic)	55.66	41.06	7987	8083
MRC (Ohmic)	56.21	41.61	8078	8176
PID (Ohmic)	56.94	41.98	8171	8270
LPG heating	7.48	12.38	14270	14290

heating methods and energy-efficient control strategies to achieve substantial reductions in carbon emissions.

Future Work

Future studies will evaluate the proposed controllers through real-time closed-loop implementation on the pilot-scale CFOH system to capture unmodelled dynamics, sensor noise and actuator limitations and to validate the simulation-based findings. Further research will concentrate on enhancing the flexibility of neural network–based controllers through online learning, hybrid control architectures and adaptive or self-tuning mechanisms to improve their robustness in response to variations in feedstock quality, environmental conditions and load changes. Additionally, multiobjective optimisation frameworks including control performance, energy consumption, economic expenditure and carbon emissions will be examined to support decision-making for environmentally sustainable operations. Subsequent research will incorporate dynamic emission factors, process variability and life cycle assessment (LCA) methodologies to provide a more comprehensive evaluation of environmental impacts. This will enhance long-term evaluations of sustainability. Finally, the scalability of smart controllers and their integration with digital twins, predictive maintenance techniques and Industry 4.0-enabled monitoring systems will be examined to facilitate real-time optimisation and improve their accessibility in sustainable thermal processing systems.

Conclusion

This study provided a comprehensive comparative analysis of NARMA-L2, model reference control (MRC) and PID controllers for the precise temperature regulation of the CFOH system, highlighting dynamic performance metrics, energy efficiency and sustainability objectives. The results indicate that NN-based controllers improve performance compared to the conventional PID controller in both transient and steady-state operations. The NARMA-L2 controller exhibited the quickest rise time, the least transient and settling time and no overshoot. This indicates enhanced responsiveness, reduced oscillations and increased stability in closed-loop mode. The MRC exhibited commendable dynamic performance and acceptable overshoot during the entire operation, but the PID controller demonstrated much longer response times, the highest overshoot and diminished stability. Despite NARMA-L2's increased energy usage during the transient phase due to its aggressive control strategy, it exhibited the lowest steady-state power consumption and the highest efficiency. This indicated that it consumed less energy over time. When implemented on a daily and annual basis, it resulted in a reduction of greenhouse gas emissions. The NARMA-L2 controller exhibited the lowest annual CO_2e emissions, followed by the MRC controller, whereas the PID controller recorded the highest emissions.

The results clearly demonstrate that advanced neural network-based controllers significantly enhance control accuracy, stability and reliability, while simultaneously improving energy efficiency and reducing associated greenhouse gas emissions under the analysed conditions. These combined benefits highlight their strong potential as effective solutions for sustainable industrial thermal processing applications. Although the present study is based on a high-fidelity, validated simulation framework, the observed performance trends provide a reliable indication of their comparative advantages. Further experimental validation under real operating conditions will further confirm their practical applicability and support their wider adoption in industrial food processing systems.

Acknowledgements The authors would like to thank Premier Foods, Ohm-E Technology (UK), and the AFIC team at Sheffield Hallam University for their guidance.

Author contributions T.J. and L.P.L. Writing - Original draft preparation; Methodology; Experimental setup; Data collection. W.I. Supervision. Validation; Writing-Review and Editing. J.S. Supervision; Validation; Writing-Review and editing. M.A. Supervision; Validation; Writing-Review and Editing. T.B. Supervision; Validation; Writing-Review and editing. C.M. Supervision; Validation; Writing-Review and Editing. M.R. Writing-Review and editing. H.Z. Supervision; Conceptualisation; Formal analysis; Resources; Writing-Review and editing. All authors have read and agreed to the published version of the manuscript.

Funding This research was supported by Innovate UK under Grant number 10074002.

Data Availability The raw data supporting the conclusions of this article will be made available by the authors on request.

Declarations

Informed Consent Not applicable.

Competing Interests The authors declare no competing interests.

References

Alamirew, T., Balaji, V., & Gabbeye, N. (2017). Design of model predictive controller for pasteurization process. *Indonesian Journal of Electrical Engineering and Informatics (IJEEI), 5*(2), 137–144.

Bachi, I. O., Bahedh, A. S., & Kheioon, I. A. (2021). Design of control system for steel strip-rolling mill using NARMA-L2. *Journal of Mechanical Science and Technology, 35*(4), 1429–1436. https://doi.org/10.1007/s12206-021-0308-7

Çelik, D., et al. (2026). Advancements in nonlinear PID controllers: A comprehensive review. *Computers & Electrical Engineering, 129*, Article 110775. https://doi.org/10.1016/j.compeleceng.2025.110775

Chebbi, A., et al. (2024). Substrate temperature estimation and control in advanced MOCVD process for superconductor manufacturing. *International Journal of Advanced Manufacturing Technology, 133*(1), 273–285.

Corigliano, O., Morrone, P., & Algieri, A. (2025). Navigating the challenges of sustainability in the food processing chain: Insights into energy interventions to reduce footprint. *Energies, 18*(2), 296. https://doi.org/10.3390/en18020296

Dinç, B., Erentürk, K. (2024) "Comparison of PID and FLC type controller designed for Ohmic heating system." In *SETSCI-Conference Proceedings.*

Dong, D., et al. (2017). "Fuzzy temperature control of induction cooker," In *IECON 2017–43rd Annual Conference of the IEEE Industrial Electronics Society.*

Elfadel Haroon, H. E. (2024) "Nonlinear auto-regressive moving average (NARMA-L2) controller design for two CSTR." In *2024 10th International Conference on Electrical Engineering, Control and Robotics (EECR).* https://doi.org/10.1109/EECR60807.2024.10607333

Fakinle, B. S., et al. (2019). Emission characterization and performance of conventional liquefied petroleum gas cookstove burners. *Cogent Engineering, 6*(1), Article 1652228.

Food & Drink Federation, Industry at a Glance. (n.d.). Available: https://www.fdf.org.uk/fdf/business-insights-and-economics/facts-and-stats/#Environmental. Accessed 20 Feb 2025

Gowreesunker, B. L., Tassou, S., & Atuonwu, J. (2018). Cost-energy optimum pathway for the UK food manufacturing industry to meet the UK national emission targets. *Energies, 11*(10), Article 2630. https://doi.org/10.3390/en11102630

Hagan, M. T., et al. (1999). Training recurrent networks for filtering and control. *Recurrent Neural Networks: Design and Applications* (pp. 311–340)

Hui, J., & Yuan, J. (2022a). Neural network-based adaptive fault-tolerant control for load following of a MHTGR with prescribed performance and CRDM faults. *Energy, 257*, Article 124663.

Hui, J., & Yuan, J. (2022b). Adaptive second-order nonsingular terminal sliding mode power-level control for nuclear power plants. *Nuclear Engineering and Technology, 54*(5), 1644–1651.

Javed, T., et al. (2025). Integrating fluid dynamics: Leveraging Simscape for modelling and real-time control of continuous flow Ohmic heater. *International Journal of Modelling and Simulation*. https://doi.org/10.1080/02286203.2025.2493660

Li, J., & Li, F. (2019). Active control of thermal buckling for plates using a temperature feedback control method. *Smart Materials and Structures, 28*(4), 045001.

MathWorks, Design NARMA-L2 Neural Controller in Simulink. (n.d.). MATLAB Deep Learning Toolbox Documentation. Available: https://www.mathworks.com/help/deeplearning/ug/design-narma-l2-neural-controller-in-simulink.html. Accessed 10 Jan 2025.

Narendra, K. S., & Mukhopadhyay, S. (1997). Adaptive control using neural networks and approximate models. *IEEE Transactions on Neural Networks, 8*(3), 475–485.

Narendra, K. S., & Parthasarathy, K. (2002). Learning automata approach to hierarchical multiobjective analysis. *IEEE Transactions on Systems, Man, and Cybernetics, 21*(1), 263–272.

Oluwole-ojo, O., et al. (2023). Energy consumption analysis of a continuous flow Ohmic heater with advanced process controls. *Energies, 16*(2), Article 868. https://doi.org/10.3390/en16020868

Oluwole-ojo, O., et al. (2024). Model validation and real-time process control of a continuous flow ohmic heater. *Modelling, 5*(3), 752–775. https://doi.org/10.3390/modelling5030040

Paul, R., & Chokkadi, S. (2016). Implementation of NARMA-L2 controller for shell and tube heat exchanger temperature process. *Industrial & Engineering Chemistry Research, 55*(19), 5644–5653. https://doi.org/10.1021/acs.iecr.5b03791

Richardson, P. (2001). *Thermal Technologies in Food Processing*. Cambridge, U.K.: Woodhead Publishing Ltd.

Skudder, P. J., Stirling, R. (1992). *The commercial development of ohmic heating processes, IEE Colloquium on Advanced Food Technology* (pp. 3/1-3/2). Runcorn, UK.

Stirling, R. (1987). Ohmic heating - A new process for the food industry. *Power Engineering Journal, 1*(6), 365–371. https://doi.org/10.1049/pe:19870065

Uddin, W., et al. (2019). A neural network-based model reference control architecture for oscillation damping in interconnected power system. *Energies, 12*(19), Article 3653. https://doi.org/10.3390/en12193653

UK Government. (2025). *Department for Energy Security and Net Zero, Greenhouse Gas Reporting: Conversion Factors 2025*. London, U.K. Available: https://www.gov.uk/government/publications/greenhouse-gas-reporting-conversion-factors-2025. Accessed 15 May 2025.

Vandoren, V. J. (1998). Open-loop control offers some advantages. *Control Engineering, 45*(13), 176.

Zhang, D., et al. (2022). Neural direct adaptive active disturbance rejection controller for electro-hydraulic servo system. *International Journal of Control, Automation, and Systems, 20*(7), 2402–2412.

Zhang, J., & Wang, M. (2023). Special issue: Neural networks, fuzzy systems and other computational intelligence techniques for advanced process control. *Processes, 11*(8), Article 2278. https://doi.org/10.3390/pr11082278